International Journal of Geosynthetics and Ground Engineering (2023) 9:54
https://doi.org/10.1007/s40891-023-00467-6

ORIGINAL PAPER

Enhancing the Mechanical and Microstructural Properties of Expansive Soils using Industrial Waste, Nano-material and Polypropylene Fibers: A Comparative Study

Mohammad Ali Pashabavandpouri[1] · Amir Reza Goodarzi[2] · Seyed Hamid Lajevardi[1]

Received: 4 December 2022 / Accepted: 1 July 2023 / Published online: 7 August 2023

Abstract
Lime is a common stabilizer in soil remediation projects. However, in terms of the considerable emissions of greenhouse gases in lime production, the replacement of environmentally friendly stabilizers with lower CO_2 emissions has attracted much attention. Accordingly, this study investigated the efficacy of expansive clay remediation employing ground granulated blast furnace slag (GGBS) and nano-metakaolin (NMK) as a substitute for lime. Moreover, polypropylene fibers (PPFs) were added to assess the simultaneous effect of the stabilization/reinforcement (S/R technique). To this end, a set of macro and micro tests including unconfined compressive strength (UCS), free swelling, electrical conductivity (EC), pH, scanning electron microscopy (SEM) analyses, X-ray diffractometer (XRD), and ultrasonic pulse velocity (UPV) were conducted on the samples cured at 20 and 40 °C after 7, 28, and 90 days of curing. The results showed that the ratio of lime to GGBS = 1:4 and replacing NMK with 20% lime as an optimum mixture (with an over 40% decline in lime consumption) increased the strength about 8.1 times that of soil and substantially limited the swelling. An important key factor that accelerated the process of improvement was higher temperature. There was a rising trend for E_{50} and E_U with increasing the additives' quantities. PPFs enhanced strength by around 11.7 times that of soil while reducing the amount of needed lime by 60%. Additionally, specimens' swelling and ductility were improved, E_U increased, and E_{50} slightly decreased. Correlations were obtained between compressive strength with E_{50} and ultrasonic pulse velocity values (UPV). XRD and SEM results confirmed increasing CSH and CAH amounts and the modification of soil's pore network by forming a denser microstructure.

Keywords Expansive soil · Lime · GGBS · Nano metakaolin · Fiber · Stabilization

Introduction

Expansive clays are susceptible to volumetric changes caused by ambient moisture changes, which can be hazardous to the long-term stability of structures [1, 2]. Therefore, it is essential to assess the swelling and strength characteristics of expansive soils, in order to avoid the post-construction collapse of structures associated with these soils [3]. In the United States, the annual loss caused by expansive soils was reported to be about $13 billion, while in Britain, it was predicted to be roughly $3 billion for ten years. The volumetric change of the expansive soil is mainly owing to the presence of the clay minerals such as montmorillonite [4–7]. Expansive soils are spread worldwide with the percentage of the total land covered by these soils in some countries given in Fig. 1 [8–14].

Numerous techniques are employed to contend with the expansive soil's swell behavior. Among all methods, chemical stabilization with conventional calcium-based stabilizer materials (CSMs) like lime and cement has gained increasing interest among researchers [9, 15, 16]. The most important reasons to use CSM by investigators in the recent past include avoiding the uneconomical replacement of these types of soils with coarse-grained materials, accelerating

✉ Seyed Hamid Lajevardi
Sh.lajevardi@iau.ac.ir

Mohammad Ali Pashabavandpouri
MA.Pashabavandpouri@iau.ac.ir

Amir Reza Goodarzi
amir_r_goodarzi@yahoo.co.uk

[1] Department of Civil Engineering, Arak Branch, Islamic Azad University, Arak, Iran

[2] Department of Civil Engineering, College of Engineering, Hamedan Branch, Islamic Azad University, Hamedan, Iran

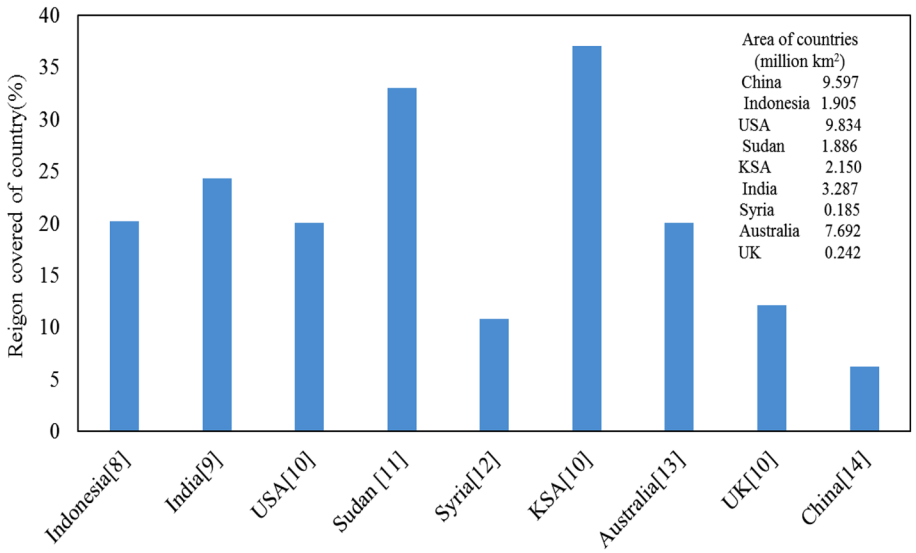

Fig. 1 The percentage of expansive soils in some countries

pozzolanic reactions and reduction of swelling due to the presence of Ca^{2+} ions, time-consuming of pre-wetting technique due to the low hydraulic conductivity of these soils, and eventually profuse availability and comparatively low cost [17]. Based on the technical literature, the reactions of stabilizers with clay minerals and the formation of cementitious products such as calcium silicate hydrates (CSH) and calcium aluminate hydrates improves soil's engineering properties [18, 19].

Many researchers have corroborated that curing conditions, such as period, temperature, and humidity, considerably affect the reactions of additives [20–23]. Salimi and Ghorbani, 2020 [24] investigated the characteristics of soft clay stabilized using slag-based blends and geopolymers at 20 and 45 °C. Rising temperature accelerates the development of cementitious products and raises UCS values, as shown by test findings [24].

Despite the remarkable effect of traditional stabilizers on soil remediation, extreme dependency on these materials entails increased energy consumption, high production expenses, and considerable emissions of greenhouse gases. The production of one ton of lime is an energy-intensive process that emits almost 0.6 to 0.82 tons of CO_2, which has catastrophic environmental effects [23]. Researchers have recently tried to take advantage of alternative pozzolanic compounds that are more affordable and eco-friendly than traditional stabilizers [18, 23, 25–28].

One of these alternatives is pozzolanic nano-materials. Nanotechnology has advanced in various fields in the last few years due to unique features [29, 30]. Nano-scale materials possess a large specific surface area and high reactivity because of their small dimensions (ranging from 1 to 111 nm). It was corroborated that nano-materials are able to change soil's physical, chemical, and mechanical properties [31, 32].

Several studies in the field of soil stabilization have been conducted on nano-silica, nano-zeolite, nano-clay, nano-MgO, and carbon nano-tube. Akbari et al. 2021 [23] assessed the effect of replacing lime with nano-zeolite in kaolinite soil. The results showed that temperature substantially accelerates reactions. The unconfined compressive strength (UCS) of stabilized specimens with 10% lime and 40% nano-zeolite was 20 times greater than the kaolinite clay. Jafari et al., 2021 [29] showed that the concurrent addition of 7% lime and 1% nano-SiO_2 leads to a substantial increase in the small strain shear modulus (Gmax) and UCS of soft clay. Yao et al. 2019 [33] examined the effects of nano-MgO and cement on the UCS and microstructure properties of soft soil. Based on the results, adding nano-MgO to the cement-stabilized soil up to the recommended optimum concentration (15%) increased the UCS and ductility and improved the microstructure. Kumar & Sinha, 2023 [34] studied the effect of multi-walled carbon nanotubes (MWCNT) and fly ash on poor subgrade soil. The soil was replaced up to 50% by fly ash in the presence of MWCNT and Sodium hexametaphosphate (SHMP) in various concentrations. According to findings 0.01% w/w MWCNT + 80% Soil + 20% Fly Ash + 2% SHMP was the optimum combination to achieve maximum UCS value. Zoriyeh et al., 2020 [35] studied the effect of nano-clay on the mechanical properties of a high plasticity soil. The results revealed that the increase in the content of nano-clay lead to an increase in UCS test results. Increasing the curing period showed a negative effect on specimens containing less than 0.5% nano-clay but it was opossite for samples with 0.5% or more nano-clay.

Despite research on nano-materials, few studies were conducted on nano metakaolin (NMK) for soil stabilization purposes. NMK emanates from the thermal activation of nano-kaolin. The NMK with ultrafine particle size, high

level of activity, and significant concentrations of silica and alumina can enhance the reactivity and generation of cementitious gels. Additionally, ultrafine NMK particles can fill nano-voids, reduce porosity, and produce a dense structure [36, 37].

Another pozzolanic material that can be substituted instead of lime and cement is ground granulated blast furnace slag (GGBS). Primarily constituting silica, calcium, aluminum, and magnesium, GGBS is a by-product in the steel industry, which investigators have used [24, 38, 39].

It is worth mentioning that using chemical additives leads to brittle behavior in treated soil [23]. According to previous studies, fibers can significantly compensate for this defect [40–44]. As a consequence, engineering properties such as swelling, strength, and durability are improved in addition to upgrading ductility [4, 45]. To reinforce the soil, researchers used a variety of natural and synthetic fibers. Polypropylene fiber (PPF) has drawn researchers' interest among all fiber types because of its exceptional mechanical properties.

To review the technical literature, a summary of the studies conducted in soil improvement using NMK, GGBS, and PPFs is listed in Table 1.

Despite a multitude of research focusing on soil remediation, the possible effect of applying nano-materials, especially NMK, to stabilize expansive soils was not adequately evaluated. Furthermore, few researches have extensively investigated the effect of simultaneous utilization of the triple additives (lime, GGBS, and NMK) with PPFs for reducing lime consumption and addressing expansive soil deficiencies. In addition, previous studies were simply interpreted regarding microstructural characteristics, particularly about nano-materials application issues in stabilized/reinforced highly expansive soil. Besides, the fundamental association between microstructural and engineering features was not comprehensively assessed based on various curing conditions.

To cover the aforementioned gaps of investigation, the present study pursues these following objectives: (1) Analyzing the efficiency of lime, GGBS, and NMK with the contribution of PPFs to improve the geotechnical characteristics of expansive soils. (2) Assessing the temperature effect on cementitious products formation and the soil remediation process. (3) Interpretation of engineering properties changes in terms of microstructural perspective in remediated smectite. (4) Examining the potential for reducing the amount of lime throughout the remediation process and determining the optimum content of additives in the stabilization/reinforcement (S/R) technique. To achieve these goals, a set of macro and micro-level tests, including UCS, free swelling, electrical conductivity (EC), pH, scanning electron microscopy (SEM) analyses, X-ray diffractometer (XRD), and ultrasonic pulse velocity (UPV) were conducted on samples cured for 7, 28, and 90 days at 20 and 40 °C.

Materials and Methods

Materials

Figure 2 depicts the particle size distribution curves and a view of used materials, including smectite, lime, GGBS, NMK, and PPFs.

Soil

The smectite (highly expansive soil) was obtained from Khorasan province is located in the north of Iran. Tables 2 and 3 include, respectively, information on the geotechnical characteristics and chemical analyses of smectite. The soil has a high concentration of montmorillonite minerals, according to the findings of the XRD test, chemical analyses, plasticity index (PI), water absorption, and swelling potential.

Nano-Metakaolin

NMK was produced by Arman Jostojugaran Energy Noor Co., Ltd, which was obtained by thermal activation (calcination) of NK at 750 °C for 2 hours. The specific surface area and bulk density of NMK are 100–150 m^2/g and 4.16 g/cm^3, respectively, with its chemical analysis given in Table 3.

Lime

Hydrated lime was used as the alkaline activator produced by Merck & Co., Inc. in Germany, with more than 96% purity, density of 2.240 g/cm^3, and solubility of 1.7 g/l. The chemical properties of lime are reported in Table 3**.**

Ground Granulated Blast Furnace Slag

GGBS was supplied by Iran's Esfahan Steel Co. as a by-product of the steel industry. The GGBS's specific gravity and specific surface area were found to be 2.81 and 4740 cm^2/g, respectively. Table 3 presents the results of the GGBS's chemical analysis. As listed in this Table, the multivalent cations at large concentrations in GBBS and NMK may be exchanged with low valence ones on the soil particle surface.

Table 1 Summary of previous studies on NMK, GGBS, and PPFs—treated soils

Author	Agents of stabilization	Optimum content	Result of treated soil after stabilization	Curing condition	Curing period	Soil type
Tiwari and Satyam [4]	PA (i.e. 5, 10, 15, and 20%) and PPF (i.e. 0.25, 0.5, and 1%.)	20% PA and 0.5% PPF	The mechanical and durability properties of soil are increased	(27 ± 2) °C and RH of 65% ± 5%	7, 14, and 28 days	Expansive soil
Shenal Jayawardane et al. [5]	CF and PPF (i.e. 0.5, 1, 1.5, and 2%) and lime 5%	5% lime and 2% CF or 1% PPF	Reduction in the swelling potential; linear shrinkage and compressibility	20 ± 1 °C and RH of 95%	7-day	Expansive soil
Akbari et al. [23]	lime (i.e. 0, 5, 10, 15, and 20%), nano-zeolite (i.e. 0, 10, 20, 30, 40, 50, 60, and 75% of lime), and PPF were 1%	10% lime with 40% replacement of nano-zeolite and 1% PPF	Compressive strength, peak strain energy (E_u), secant modulus (E_{50}), tensile strength, and strain of the samples increased	20 and 40 °C with a RH of 85%	7, 28, and 90 days	Soft soil (kaolinite clay)
Salimi and Ghorbani [24]	Slag (GBFS and BOFS) and Activator (CaO and MgO). Binders (i.e. 2.5, 5, 10, and 20%.). Na_2SiO_3:NaOH (i.e. 100:0, 80:20, 60:40, 40:60, 20:80, and 0:100.)	The activator to slag ratio was 1:3. additives 20% and Na_2SiO_3:NaOH ratio of 80:20	The increasing temperature led to a faster formation of cementitious gels; The UCS values of the MB and CB samples increased in Na_2SiO_3:NaOH ratio of 80:20	20 and 45 °C with a relative humidity of 85%	7, 28, and 90 days	Soft soil (kaolinite clay)
Akbari et al. [43]	lime (i.e. 0, 5, 10, and 15%), nano-zeolite (i.e. 0, 10, 20, 30, 40, 50, 60, and 75% of lime), PPF (i.e. 0, 0.5, 0.75, 1 and 1.25% of dry mass)	Replacement of 40% lime with nano-zeolite and 1% PPF	Major reduction in lime consumption; an increase in compressive strength; an improvement in durability against wet-dry conditions	20 and 40 °C with a RH of 85%	7, 28, and 90 days	Soft soil (kaolinite clay)
Goodarzi and Salimi [56]	GBFS and BOFS with 2.5, 5, 10, 15, 20, and 30% in soil dry mass	BOFS(10%) and GBFS(20–25%)	The elimination of soil dispersion; With increasing the curing time, the strength improves	22 ± 1 °C with a RH of 85%	1, 3, 7 and 28 days	Expansive soil
Sharma & Sivapullaiah [57]	GGBS (30%), FA/GGBS ratio was 7:3 and Binder was 0,10,20,30 and 40%	Binder: 40%	Reduction in compressibility features; Further reduction in swelling and compressibility by adding 1% of lime to the mixture	Room temperature	28 days	Expansive soil

Table 1 (continued)

Author	Agents of stabilization	Optimum content	Result of treated soil after stabilization	Curing condition	Curing period	Soil type
Mohantyet al [58]	GGBS (i.e. 0, 5, 10, and 15%), cement(0 and 30%), and FA (i.e. 0, 5,10, and 20%)	Mixing of 20% FA, 15% GGBS and 30% cement	Decrease in soil dispersion and enhancement of strength; The formation of more hydrated compounds based on XRD tests; Improvement of durability against the freeze–thaw cycles	Room temperature	7, 14, 28, 60 and 90 days	Dispersive soils
Zhang et al. [59]	Cement (12 and 15%) and MK (i.e. 0, 1, 3, and 5%)	MK 5% and Cement 12%	The UCS improved; Obtaining sufficient strength in early curing process; Changing the pore volume distribution with the filling effect	20 ± 2 °C with a RH of 95%	7 and 28 days	Expansive soil
Khadka et al. [19]	MK and FA (i.e. 6, 9, 12, 15, and 18%) by mixing Na2SiO3:NaOH	Additives concentration in the range of 6.0–9.5% of the geopolymer	Improvement through geopolymer showed minimum swell and the ettringite did not form in samples	23 °C with a RH of 40%	7 days	Expansive soil
Rajabi and Hamrahi [60]	MK with 2, 5, 10, 15, 20, and 25%	MK: 25%	Increase in strength; Diminishing hydraulic conductivity; Reducing the maximum specific dry weight of soil; Increasing optimal water content	20 ± 2 °C	7, 14, and 28 days	Clayey sand soil
Abdi et al. [48]	1%, 3% and 5% lime; 0.1% PPFs	5% lime and 0.1% PPF	Adding PPF to mixture improves ductility, increase compressive and shear strength; Lime content and curing period were influential factors	35 °C with a RH of 90%	1, 7, and 28 days	Kaolinite

Table 1 (continued)

Author	Agents of stabilization	Optimum content	Result of treated soil after stabilization	Curing condition	Curing period	Soil type
Miraki et al. [52]	VA/GGBS ratios (i.e. 100/0, 85/15, 70/30, 55/45, and 0/100). The total binder content was fixed at 20% of the soil mass	VA/GGBS ratio:70/30	The low carbon footprints by replacing VA with GGBS; Unlike the samples with 0% GGBS, the combination of VA and GGBS showed enough strength against W-D cycles; Temperatures had a significant effect on the formation of cementitious gels	25 ± 5 and 65 °C with a RH of 80% + 2%	7, 28, and 90 days	Clayey soil (CL)

GBFS granulated blast furnace slag, *BOFS*: basic oxygen furnace slag, *PA* pond ash, *FA*: fly ash, *PPF*: polypropylene fiber, *CF*: natural coir fibers, *CaO* calcium oxide, *MgO* medium reactive magnesia, *RHA* rice husk ash, *GGBS* ground granulated blast furnace Slag, *MK* metakaolin, *RH*: relative humidity, *VA* = volcanic ash, *W-D*: wet-dry cycles

Polypropylene Fiber

Due to their lower cost and superior mechanical application compared to other fibers, researchers believe PPFs to be more effective [46, 47]. They demonstrated that the ideal length for soil reinforcement is 12 mm, which has a tolerable influence on lime-stabilized clay [23, 48]. Therefore, this length was considered for PPFs in this study. The physical and mechanical properties of PPFs are given in Table 4.

Mix Proportion

The smectite was remediated with different amounts of GGBS and NMK using lime as an activator (Table 5). To this end, the appropriate ratio of lime to slag was determined in the first step. Previous studies showed the optimum ratio of the activator to the slag was 1:3 [24, 39] and 1:5 [49]. Additives with various lime-to-GGBS ratios, including 1:5, 1:4, and 1:3, were added to the soil, cured at 40 °C for 28 days, and then tested. Since the UCS value (Fig. 3) associated with the ratio of 1:4 was close to 1:3 (the difference was less than 10%) and one of the goals of this study is to reduce lime consumption, so the ratio of lime to GGBS = 1:4 was taken into consideration. In the next step, NMK was replaced with 0, 20, 40, and 60% lime in the mixtures. At last, various percentages of blends, including 0, 5, 10, 15, and 20%, based on the dry weight of the soil, were added to the smectite. Then the required quantity of water equal to the optimum moisture content (see Table 5) was added to the resulting mixtures and thoroughly mixed to obtain homogenous mixes.

To make comprehending the combination percentage easier to grasp, Table 5 is provided. For instance, the 10(20NMK) combination denotes the sample in which NMK was substituted for 20% of the lime, and the 10 represents the percentage of this compound that was added based on the dry weight of the soil.

It is worth noting that the materials were dried in the oven at 105 °C for 24 h to evaporate any absorbed water, then passed through No. 200 sieve.

To assess the effect of fiber and determine the optimum content, different percentages of PPFs, including 0, 0.25, 0.5, 0.75, 1, 1.25, and 1.5 were added to mixtures. The UCS results indicated that the sample's strength increased up to adding 1% fibers and then decreased. Moreover, previous studies have confirmed that using 1% PPFs improves soil properties [23, 43, 50, 51]. Therefore, 1% (as the optimum content) of fiber was added to the mixtures.

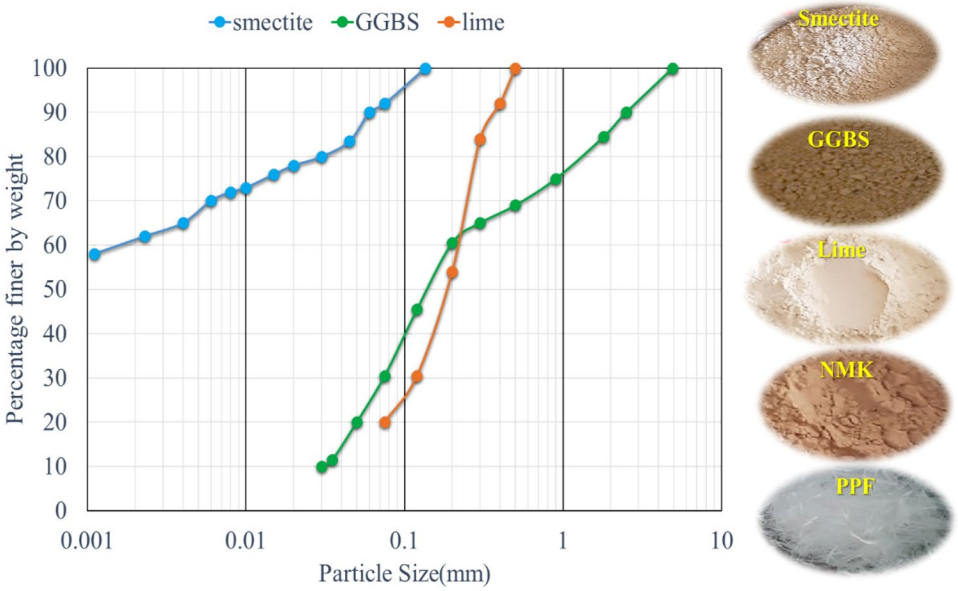

Fig. 2 Particle size distribution curves and a view of materials

Table 2 The geotechnical properties of the Smectite

Soil properties	Value	Standard designation
Cation exchange capacity (cmol kg^{-1})	81	ASTM D7503-18
Clay fraction (%)	75	ASTM D 422
Liquid limit (%)	325	ASTM D 4318
Plastic limit (%)	42	ASTM D 4318
Plasticity index (%)	283	ASTM D 4318
Specific gravity, GS	2.74	ASTM D 854
Maximum dry density (g/cm^3)	1.36	ASTM D 698
Optimum moisture content (%)	39	ASTM D 698
Swelling potential (%)	148	ASTM D 4546
Soil classification	CH	ASTM D 2487
Unconfined compressive strength (MPa)	0.48	ASTM D 2166
pH	10.53	Akbari et al., 2021[23]
Electrical conductivity (mS/cm^{-1})	2.8	Akbari et al., 2021[23]

Table 3 Chemical compositions of materials based on X-ray fluorescence (XRF)

Composition	Content (%)			
	Smectite	NMK	GGBS	Lime
SiO_2	61.9	61.3	35.14	0.2
Al_2O_3	15.5	31.2	13.67	0.1
Fe_2O_3	0.5	0.24	1.12	0.2
CaO	2.2	0.43	34.77	96
MgO	3.3	0.09	7.42	0.8
Na_2O	2.34	0.26	0.47	–
K_2O	0.92	0.06	0.55	0
P_2O_5	0.08	–	–	–
CL	0.25	–	–	–
SO_3	–	0.05	2.54	0.6
TiO_2	0.12	0.09	1.28	–
Loss on ignition	12.89	6.28	3.04	1.9

Specimen Preparation and Test Plan

The test programs are given in Table 5. According to Akbari et al., 2021 [23], the EC and pH tests were conducted to interpret the results. To this end, the blends were mixed with distilled water with a soil–additive to water ratio of 1:20. Then, prepared suspensions were shaken entirely by a horizontal vibrator to reach equilibrium. The EC and pH values were recorded after 1, 3, 7, 28, and 90 days.

For the UCS test, the homogeneous mixtures were poured into a steel cylinder with 37 mm diameter and 74 mm height and then compacted by a hydraulic jack to obtain the maximum dry density (MDD) of each mix in Table 5.

Table 4 Properties of PPFs

Properties	Value
Modulus of elasticity (MPa)	2700
Resistance to acids, alkalis, and salts	High
Melting point (°C)	160–170
Tensile strength (MPa)	350
Diameter (μm)	19 ± 2
Density (g/cm^3)	0.91
Length (mm)	12
Elongation (%)	80

Table 5 The proportion of materials and testing program

Mixture	Additives	Lime to GGBS	NMK Replacement with lime	Additives content in the mixture (%)			MDD (kg/m^3)	OMC (%)	Testing program
				Lime	GGBS	NMK			
Smectite	0	0	0	0	0	0	1360	39	SP, FSI, UCS, SEM, XRD, XRF, EC, pH, COM, UPV
5(0NMK)	5	1:4	0	1	4	0	1298	41.7	UCS, COM, FSI, UPV
5(20NMK)	5	1:4	20	0.8	4	0.2	1310	41.2	SP, FSI, UCS, EC, pH, UPV
5(40NMK)	5	1:4	40	0.6	4	0.4	1319	40.8	UCS, COM, FSI, UPV
5(60NMK)	5	1:4	60	0.4	4	0.6	1327	40.1	UCS, COM, FSI, UPV
10(0NMK)	10	1:4	0	2	8	0	1221	43.3	UCS, COM, FSI, UPV
10(20NMK)	10	1:4	20	1.6	8	0.4	1242	42.9	SP, FSI, UCS, EC, pH, UPV
10(40NMK)	10	1:4	40	1.2	8	0.8	1263	42.2	UCS, COM, FSI, UPV
10(60NMK)	10	1:4	60	0.8	8	1.2	1281	41.7	UCS, COM, FSI, UPV
15(0NMK)	15	1:4	0	3	12	0	1173	45.8	UCS, COM, FSI, UPV
15(20NMK)	15	1:4	20	2.4	12	0.6	1201	44.4	SP, FSI, UCS, EC, pH, UPV
15(40NMK)	15	1:4	40	1.8	12	1.2	1219	43.5	UCS, COM, FSI, UPV
15(60NMK)	15	1:4	60	1.2	12	1.8	1232	43	UCS, COM, FSI, UPV
20(0NMK)	20	1:4	0	4	16	0	1131	47.9	UCS, COM, FSI, UPV
20(20NMK)	20	1:4	20	3.2	16	0.8	1175	46.3	SP, FSI, UCS, EC, pH, SEM, XRD, UPV
20(40NMK)	20	1:4	40	2.4	16	1.6	1191	45.1	UCS, COM, FSI, UPV
20(60NMK)	20	1:4	60	1.6	16	2.4	1206	44.2	UCS, COM, FSI, UPV

UCS unconfined compressive strength, *SP* swelling pressure, *FSI* free swelling index, *SEM* scanning electron microscope, *XRF* X-ray fluorescence, *XRD* X-ray diffraction; *COM* = compaction, *EC* electrical conductivity; and *UPV* ultrasonic pulse velocity

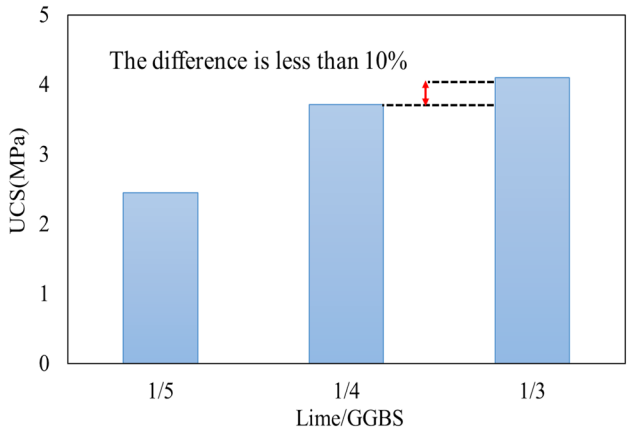

Fig. 3 UCS values of samples with different ratios of lime: GGBS cured at 40 °C for 28 days

Immediately after removing the samples from the mold, they were wrapped in multi-layer nylon bags to prevent water evaporation. They were next cured in the Germinator machine at 20 and 40 °C for 7, 28, and 90 days with a relative humidity of 85%. The samples' strength was evaluated based on ASTM D 2166 standard after curing at a constant strain rate of 1.2 mm/min. To simulate room temperature and warm regions conditions, respectively, curing at 20 and 40 °C was followed. Moreover, many researchers confirmed the effect of higher temperatures on the acceleration of pozzolanic reactions [20–24, 43, 52]. Therefore, mentioned temperatures were considered to assess curing temperature effects on reactions and obtaining practicable results on soil stabilization in different temperature conditions worldwide.

Following the curing period, the samples' one-dimensional free swelling was measured using an oedometer apparatus in accordance with ASTM D4546. The homogeneous mixtures were compacted in the rings with 50 mm diameter and 20 mm height. Up until swell-time equilibrium was reached, the free swelling index (FSI) values were recorded at elapsed time intervals.

SEM and XRD were conducted to study the specimens' mineralogical and microstructural behavior. SEM images were magnified 3000 times using an electron electroscope with a VEGA2-TESCAN model, and XRD analyses were conducted in the range of 2θ, from 4 to 60 degrees.

In the last steps of tests program, the ultrasonic pulse velocity (UPV) test was conducted to assess the results more accurately, and the relationships between UCS and UPV were given.

It is worth mentioning that all experiments were repeated in triplicate for each blend, then average results were calculated to minimize variations and ensure consistency.

Results and discussion

Effect of Additives on the UCS Test

Figure 4 shows the variations of UCS test results with the curing periods of 7, 28, and 90 days at 20 and 40 °C. Based on the results in Figs. 4a, b (non-fibers samples), compared with 20 °C, the pozzolanic reactions at 40 °C enhance the samples' strength more significantly due to the quick production of cementitious gels via the reaction of Si^{4+} and Al^{3+} ions with the Ca^{2+} (Eqs. 3, 4). Besides

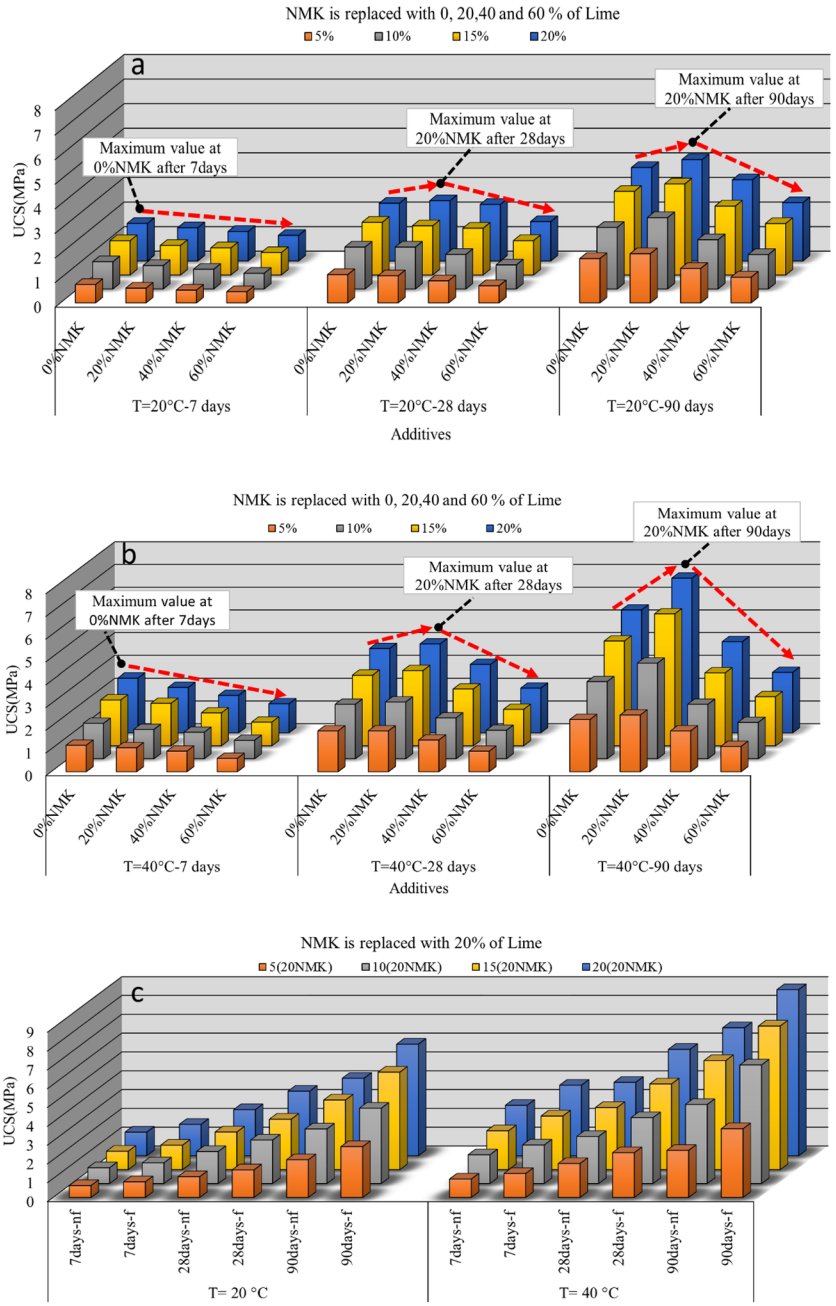

Fig. 4 UCS values of stabilized samples after 7, 28, and 90 days; **a** non-fibers at 20 °C; **b** non-fibers at 40 °C; **c** Comparison between samples with fibers (**f**) and non-fibers (nf) at 20 and 40 °C

temperature, another crucial factor affecting strength is curing time. The more prolonged curing time increases the strength when there are sufficient raw materials and moisture.

The improvement of soil engineering properties through chemical materials is known as short-term and long-term (pozzolanic) reactions. Cation exchange and flocculation occur in terms of short-term reactions. Cementitious agents, such as CSH and CAH gels, are generated in terms of long-term reactions. The mechanisms of reactions are given in Eqs. 1–4.

$$CaO + H_2O = Ca(OH)_2 \quad \text{Hydration of quicklime} \tag{1}$$

$$Ca(OH)_2 = Ca^{2+} + 2(OH)^- \quad \text{Ionization of calcium hydroxide pH rises to about 12.4} \tag{2}$$

$$Ca^{2+} + 2(OH)^- + SiO_2 = 3CaO\ 2SiO_2\ 3H_2O \quad \text{Calcium Silicate Hydrate (CSH)} \tag{3}$$

$$Ca^{2+} + 2(OH)^- + Al_2O_3 = 3CaO\ Al_2O_3\ 3H_2O \quad \text{Calcium Aluminate Hydrate (CAH)} \tag{4}$$

The cementitious gels (Eqs. 3, 4) extend the engagement, bonding, and interlocking of particles, filling the pores and raising the strength remarkably [23].

The findings in Figs. 4a, b reveal that samples without NMK and 20% NMK replacement at 20 and 40 °C, respectively, for 7-day samples and 28 and 90-day samples exhibit greater strength than substitutions of 40% and 60%. Therefore, a content of 20% NMK substitution can be thought of as optimum for 28 days of curing. This issue can be explained as follows:

(1) On the one hand, the absence of NMK (with high reactivity features) leads to a decrease in the content of reactants (SiO_2 and Al_2O_3) for reacting with $Ca(OH)_2$. Therefore, the lower amounts of cementitious agents can be produced in the samples without NMK.
(2) On the other hand, regarding a decline of lime content in 40 and especially 60% replacement, the low concentration of $Ca(OH)_2$ may not fully activate and dissolve the raw materials to increase strength, resulting in a part of the materials remaining unreacted and ineffectual. In fact, using the appropriate amount of lime, NMK, and GGBS in a 20% replacement, more Si^{4+} and Al^{3+} ions are released and quickly polymerize with Ca^{2+} under the effect of electric charge. As a result, free lime is consumed more quickly, and more adhesive gels are formed. This issue is later supported by XRD and SEM results in Sect. "Mineralogical and microstructural characteristics".

The chemical reaction mechanism of lime, NMK and GGBS is shown in Fig. 5a. In the main phase, the incorporation of additives to soil in appropriate content, leads to the dissolution of alumino-silicates of raw materials (GGBS and NMK) with the presence of hydroxyl ions in alkali-ambient. Then the dissolved Si and Al complexes move in order to condense with alkali cations (polycondensation) which leads to gel formation and reorganization. Cementitious compounds are eventually created in the final phase as a result of the polymerization and crystallization of the formed gels [13].

Since the NMK replacement with 20% lime showed better UCS results, the mixtures including 5(20NMK), 10(20NMK), 15(20NMK), and 20(20NMK) were selected as the optimum content (highlighted in Table 5).

Figure 5b is provided to compare the activator concentration (lime) in the optimum mixtures, such as 15(20NMK) and 20(20NMK), with the samples treated with lime alone. After 28 days of curing at 40 °C, the unreinforced 15(20NMK) and 20(20NMK) had UCS values of 3.30 and 3.9 MPa (8.1 times soil strength), respectively. These values are equivalent to the strength of stabilized samples with 4 and 5.8% lime after 28 days of curing. Notably, the lime content of 15(20 NMK) and 20(20 NMK) are 2.4 and 3.2% (see Table 5). Thus, consumed lime of these mixtures compared to the 4 and 5.8% lime-soil was reduced by more than 40%.

Although stabilized soils with additives are stronger than untreated soils, they are more brittle, and the formation of tensile cracks is often dominant failure pattern [23]. Therefore, the optimum content of PPFs (1%) was added to stabilized samples to compensate for this defect. Figure 4c demonstrates the UCS test results of reinforced optimum mixtures with 1% fiber cured at 20 and 40 °C for 7, 28, and 90 days. The findings show that using fibers and additives simultaneously boosted the specimens' compressive strength by around 30 to 50% when compared to samples without fibers. In general, fibers with three mechanisms improve the strength of the system:

(i). PPFs possess considerable high tensile resistance, therefore, at the fibers-soil particles interface with the contribution of cementitious gels, they can be more resistant to pull out. Therefore, the samples fail at higher compressive forces during the UCS test as a consequence of increased mobilization of tensile forces in fibers (Fig. 5c). It should go without saying that, increased curing time and temperature result in the production of more cementitious gels, which increases binding strength and adhesion at the fiber-soil particle interface. In Fig. 4c, at 40 °C, the 28-day reinforced compressive strength of 15(20NMK) and 20(20NMK) samples are 4.52 and 5.66 MPa (about 11.7 times greater

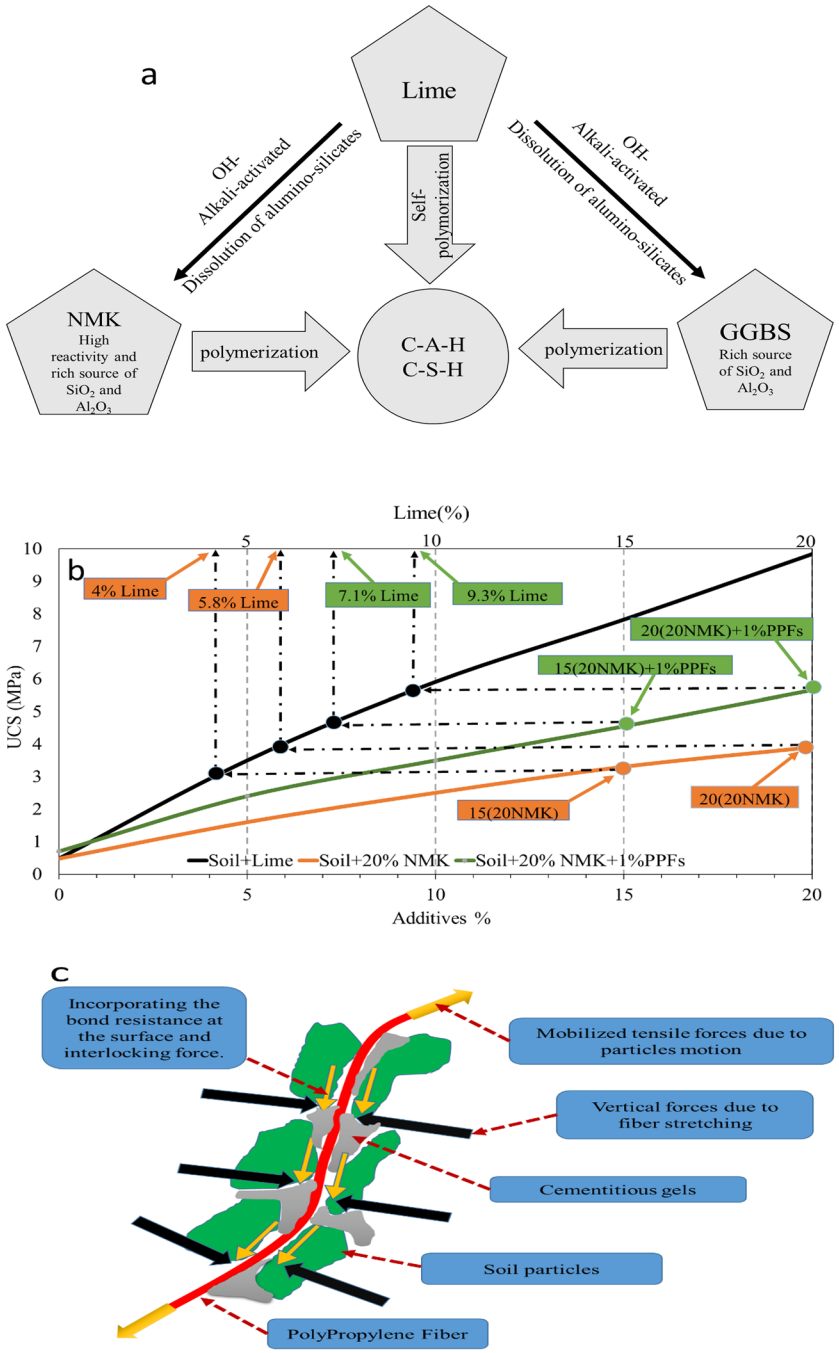

Fig. 5 **a** Chemical reaction mechanism of lime, NMK and GGBS, **b** The comparison of lime consumption in samples with fibers and non-fibers with samples stabilized by sole lime, **c** A schematic view of the fibers' reinforcement mechanism

than the smectite). However, they were 2.68 and 3.44 MPa at 20 °C, respectively.

(ii). When the external load increases, fibers are more stretched, and their curvature increases the particles' compression. This factor increases normal stress on the slip surface, leading to higher shear strength (Fig. 5c).

(iii). Fibers generate a spatial string network that restricts particle motions. In other words, the reinforcers can upgrade the system's cohesion and play a role almost similar to the spatial confinement effect.

To assess the reduction of lime consumption, a comparison between reinforced samples and treated specimens with lime alone is given in Fig. 5b. The UCS values of reinforced 15(20NMK) and 20(20NMK) cured at 40 °C after 28 days are equivalent to adding 7.1 and 9.3% lime to the soil in the same curing time, respectively. Since the used activator in 15(20NMK) and 20(20NMK) blends is 2.4 and 3.2% (see Table 5), the consumed lime, compared to the 7.1 and 9.3% lime-soil samples, is reduced by more than 60%.

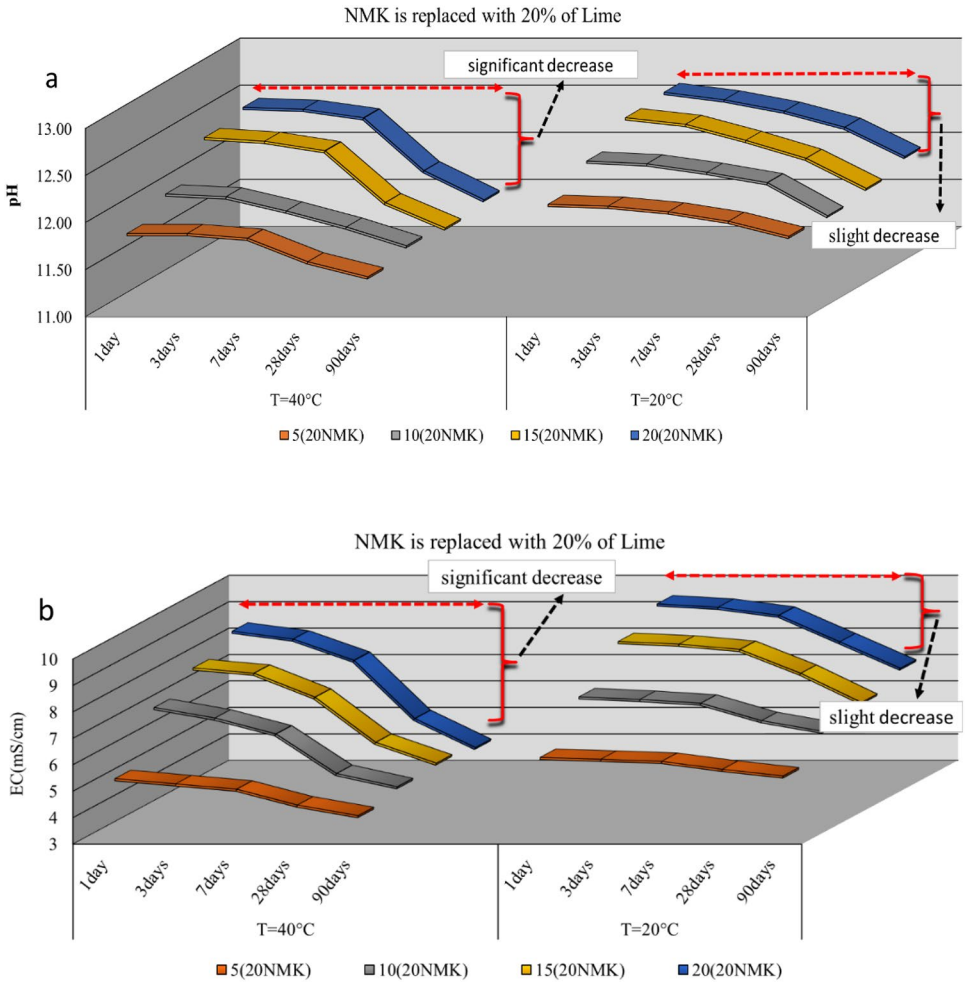

Fig. 6 Effect of additives on the pH and EC values of samples cured at 20 and 40 °C

Effect of Additives on The pH and EC

The pH and EC test results on optimum mixtures are presented in Fig. 6 at two different curing temperatures. According to the results, at the beginning of experiment, the increase in pH was higher at 20 °C. For example, after one day, at 40 °C for 20(20NMK), the pH from 10.53 for smectite raised to 12.46. However, at 20 °C, it was 12.55.

Based on the results, after 90 days at 40 °C, the pH values are lower than they were at 20 °C, and the reduction slope steepens over time. As a consequence, higher temperatures promote reactions that lead to increased CaO consumption and rising UCS values. In other words, as time passes, less unreacted CaO in samples causes the pH at 40 °C to decrease even more. It is interesting to note that the unused free lime in the system makes possible the formation of swollen minerals such as ettringite and thomosite (if exposed to sulfate conditions), which causes post-instability problems in lime-stabilized soil [23].

Findings show, one of the most potent agents that impact the behavior of stabilized samples is the higher curing temperature, affecting the reaction's acceleration. These outcomes aligned with the UCS test results and acknowledged the high strength of optimum mixtures at 40 °C.

In Fig. 6b, the EC value for 20(20NMK) from 2.8 mS/cm for smectite reached 8.8 mS/cm after one day at 40 °C, while at 20 °C, it was 9.43 mS/cm. The dissolution of lime in treated soil has increased calcium and hydroxyl ions, which explains the rising EC at the beginning of test [21]. In the dual dispersion layer of smectite particles, the base cations exchange between the monovalent ions, and across materials, the cations with greater capacity replace those with lower capacity. Consequently, the concentration of the polyvalent cations in the pore fluid among particles is enhanced [18].

The results show that EC values of samples at 40 °C compared to 20 °C experienced higher decline rates and demonstrated the least amount within 90 days. These reductions can be related to the advance in chemical reactions between materials and more consumption of ions over time.

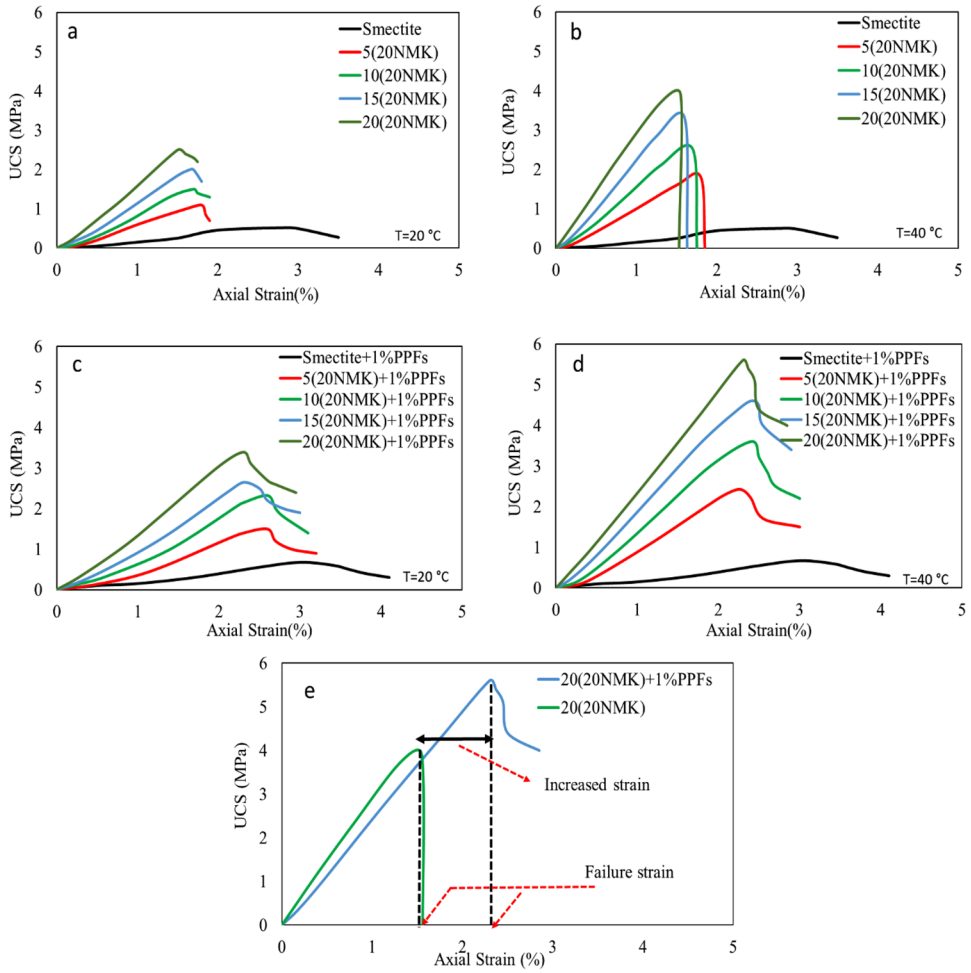

Fig. 7 Stress–strain curves of 28-day samples (NMK is replaced with 20% Lime) cured at 20 and 40 °C. **a** and **b** Non-fibers; **c** and **d** With 1% PPFs; **e** The comparison of failure strain between non-fibers and fiber-reinforced samples

Effect of Additives on the Stress–Strain

The stress–strain diagrams of 28-day samples without fibers (a and b) and reinforced with 1% PPFs (c and d) are shown in Fig. 7. The accomplishment of pozzolanic reactions, especially at higher temperatures, results in the brittleness and rapid failure of unreinforced specimens. The strain is not apparent in these samples after the maximum stress point, and they show hardening behavior (Fig. 7b). However, specimens at 20 °C show slight strain and minor ductile failure (Fig. 7a).

During the UCS test, it was observed that smectite failed with a bulging failure mechanism under axial compressive force (Fig. 8a). Adding pozzolanic materials to the soil leads to brittle failure and complete demolition in the specimens cured at 40 °C (Fig. 8b). Moreover, the shear failure pattern happened in the samples cured at 20 °C due to more moisture content and lower strength (Fig. 8c).

Figures 7c and d show the results of the PPFs inclusion in stabilized samples. As evident in the stress–strain curve, the specimens' post-peak behavior emanates from the presence of fibers, and diminishes brittle behavior. As a result, failure strain in reinforced specimens is much higher (around 40 to 60%) than in non-reinforced samples (Fig. 7e). By retaining the surrounding particles, PPFs act as a bridge surface that can endure tensile forces caused by an increasing crack width under loading and limit the creation or extension of the crack width [53].

When cracking happens, the fibers can transfer stresses by bridging two sides of cracks. As a result, strain increases (Fig. 8d). In the first step, they act as inhibitors for extending micro-cracks generated at low strains. With rising strain and extended width of cracks, the loads carried by the soil matrix are transferred to the reinforcement elements and distributed locally. Then the generated tensile forces in fibers are shifted back to the soil matrix again by a shear-lag mechanism, leading to the uniformity of macro cracking. Accordingly, the fibers can play a more prominent role in emerging ductile behavior at high strain levels.

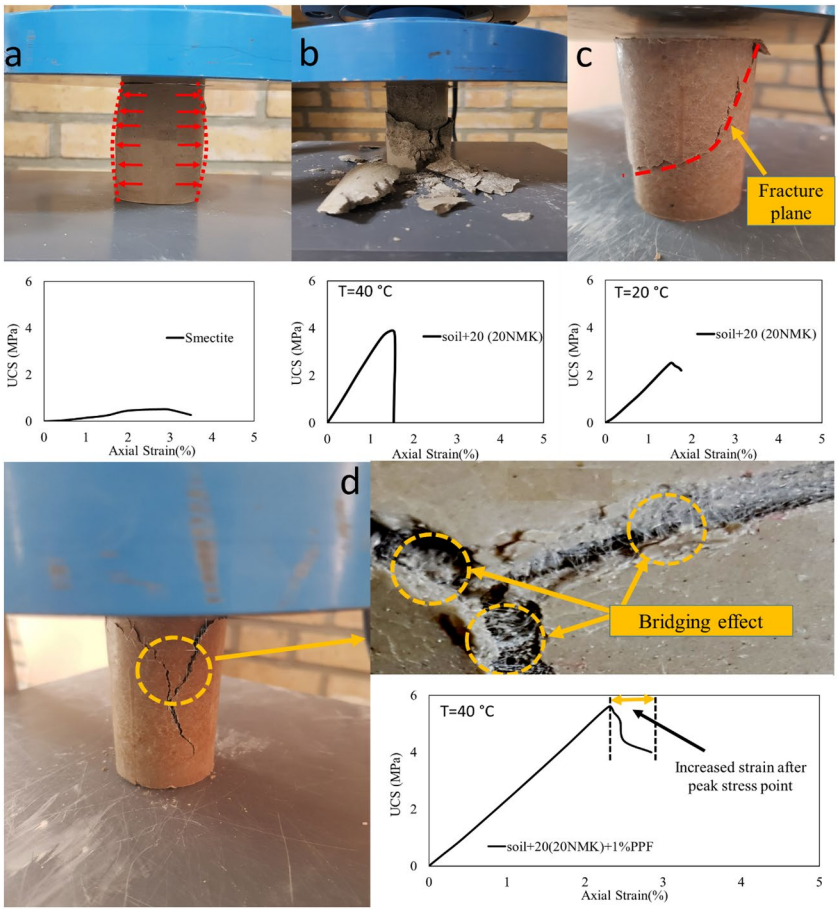

Fig. 8 Failure patterns of samples after 28 days. **a** Smectite; **b** 20(20NMK) cured at 40 °C; **c** 20(20NMK) cured at 20 °C; **d** 20(20NMK) reinforced with PPFs, cured at 40 °C

Effect of Additives on the Peak Strain Energy (Eu) and Secant Modulus (E_{50})

The peak strain energy (Eu) is a significant parameter to assess the impact of additives on the samples' toughness. Peak strain energy, also known as energy absorption capacity, is the quantity that can be determined by computing the area under the stress–strain curve up to the maximum stress [24]. In the stress–strain curve, the slope of a straight line connecting the origin to half of the failure stress point is the secant modulus (E_{50}), indicating the stiffness or flexibility of specimens [43].

Figure 9 demonstrates the Eu and E_{50} related to the stress–strain curves (Fig. 7) of fibers and non-fibers samples after 28 days at 20 and 40 °C. Based on the diagrams increasing the binders percentage and curing temperature cause enhancement of Eu and E_{50}. Since, treated samples experience higher UCS values, thus stress of the rupture point and the area beneath the stress–strain curve increase. For instance, the Eu and E_{50} values of unreinforced 20(20NMK) at 20 °C are 24.26 kJ/m^3 and 176.69 MPa (Fig. 9a) while, at 40 °C, they are 35.66 kJ/m^3 and 294.47 MPa, respectively (Fig. 9b).

Compared to non-fibers samples, Eu values increase with the strength enhancement for the fiber-reinforced specimens (Figs. 9c, d). It means the needed energy to rupture at higher stress in the fiber-containing samples was greater. On the other hand, as concluded from the stress–strain curves (Fig. 7), the specimens' ductility is raised using elastic fibers, which causes increasing failure strain, and a minor decline in E_{50}. For instance, the Eu and E_{50} at 40 °C achieved 35.66 kJ/m^3 and 294.47 MPa, respectively, in the unreinforced 20(20NMK) sample (Fig. 9b). For the reinforced specimen, they were 83.2 kJ/m^3 and 248.5 MPa, respectively, under the same curing conditions (Fig. 9d).

The best fits based on the data were performed to elucidate the numerical relationships between UCS and E_{50} results in Eqs. 5 and 6 are obtained from Fig. 10.

$$E_{50}(\text{MPa}) = -2.0134UCS^2 + 73.71UCS - 18.023\text{and}R^2 = 0.9287\text{unreinforcedsamples} \quad (5)$$

$$E_{50}(\text{MPa}) = 3.5719UCS^2 + 23.657UCS + 13.427\text{and}R^2 = 0.9441\text{unreinforcedsamples} \quad (6)$$

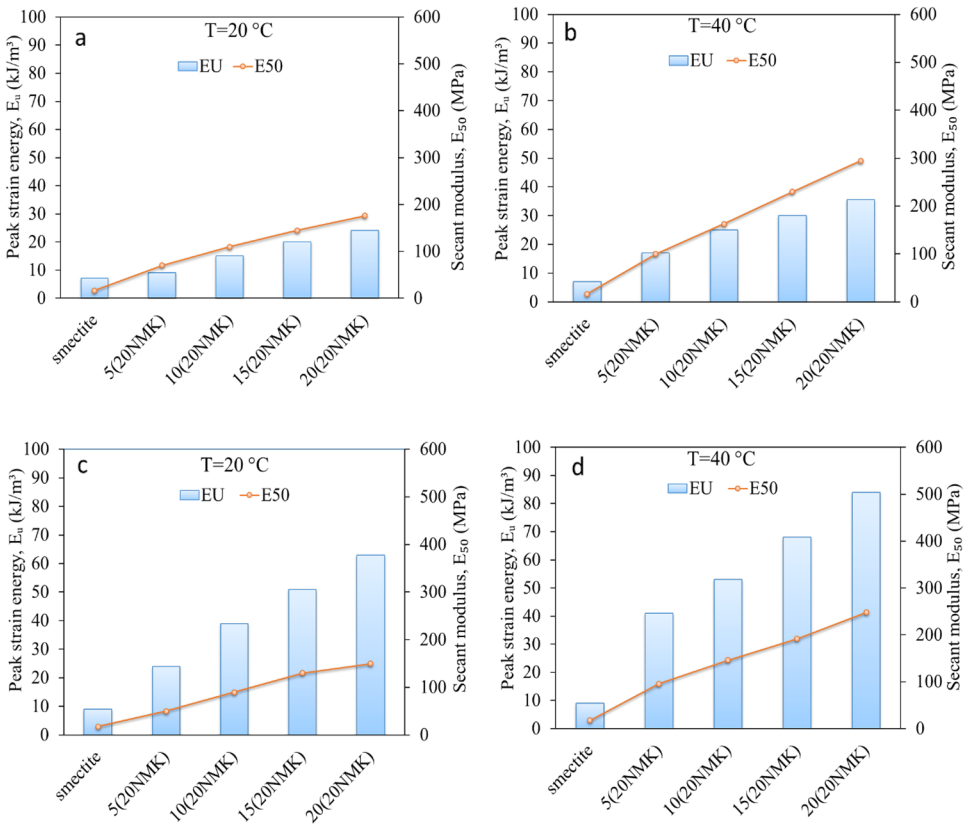

Fig. 9 Eu and E50 values of 28-day samples (NMK is replaced with 20% Lime). **a** and **b** Without fibers; **c** and **d** With 1% PPFs

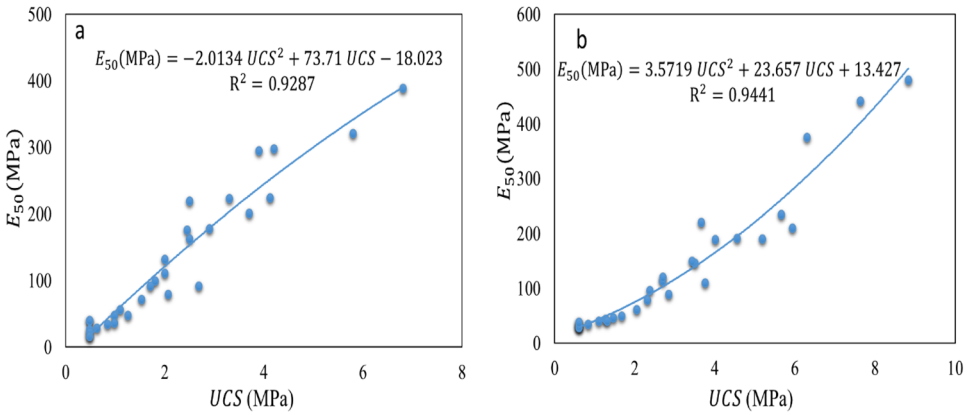

Fig. 10 Relationships between E50 and UCS values. **a** Without fibers. **b** With 1% PPFs

Equations (5) and (6) have relatively acceptable correlation coefficients (R^2) and can be helpful for preliminary assessments.

Effect of Additives on the Swell Characteristics

The free swelling index (FSI) of samples at ultimate heave was calculated as the proportion of excess in thickness (ΔH) to initial thickness (H), which is expressed as a percentage based on Eq. (7). Moreover, after measuring the ultimate heave, the sample was subjected to increasing vertical pressure until the initial void ratio (e_0) was obtained. Therefore, it was possible to determine swelling pressure (Ps).

$$\text{FreeSwellingIndex(FSI)} = \left(\frac{\Delta H}{H}\right) \bullet 100 \tag{7}$$

The result of free swelling test for different replacements of NMK is given in Fig. 11. As was shown, the minimum value of FSI for 7-day samples was related to 0% NMK. However, the lowest amount was 20% replacement after 28 days. The results are in line with the UCS test trend in Sect. "Effect of additives on the UCS test",

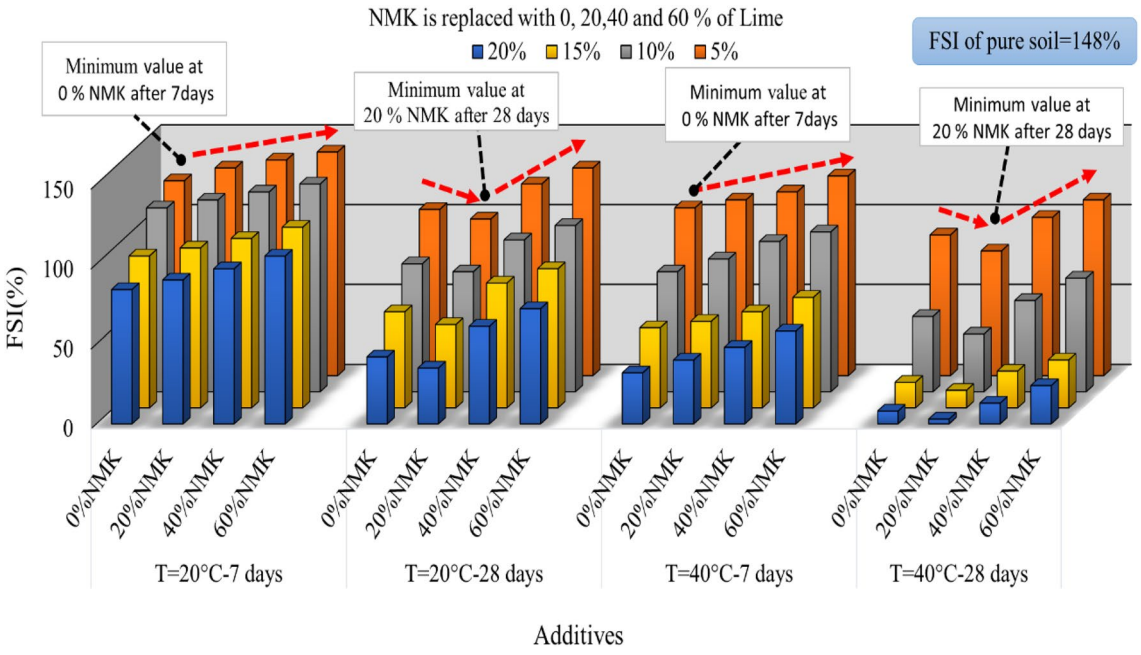

Fig. 11 FSI of non-fiber samples cured for 7, 28 days at 20 °C and 40 °C

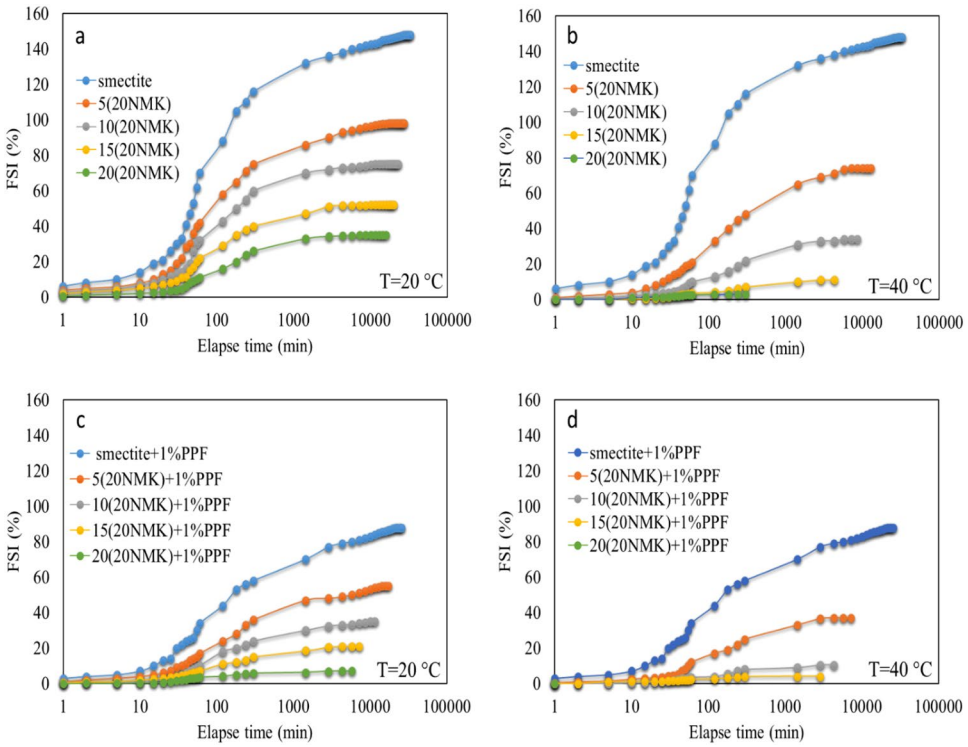

Fig. 12 FSI of samples, cured at 20 and 40 °C for 28 days (NMK is replaced with 20% Lime). **a** and **b** Non-fibers; **c**, **d** With 1% PPFs

and it can be assumed that 20% NMK replacement is the optimal amount to reduce swelling.

Figure 12 depicts the changes of FSI versus elapsed time for optimum replacement, which were cured at 20 and 40 °C for 28 days. The FSI of untreated soil reached 148% during 21 days. By adding chemicals to unreinforced samples, besides the significant decline in FSI, the elapsed time for the ultimate heave was reduced (Figs. 12a, b). Since cementitious compounds form quickly at higher temperatures, this issue is more validated for samples that have been cured at those temperatures. For example, at 20 °C, FSI for 20(20NMK) after 11 days reached

35% (Fig. 12a), while at 40 °C, it was 3% after one day (Fig. 12b).

Regarding reinforced samples (Figs. 12d, c), swelling reduction depends on the curing temperature and the content of additives. Because with the increase of both factors, more sticky gels are produced, the binding of fibers to soil particles improves, and as a result, volumetric changes are controlled more quickly. For instance, at 20 °C, the FSI for reinforced 15(20NMK) after seven days reached 21% (Fig. 12c), while at 40 °C, it was 4% after two days (Fig. 12d).

Figures 13 a and b show the concurrent results of FSI and swelling pressure for optimum mixture, after 7, 28, and 90 days of curing, at 20 and 40 °C. Results on smectite showed that the ultimate swelling pressure (equivalent to FSI = 148%) was increased as high as 1776 Kpa, which is indicated the structures on this problematic soil are at risk of severe and permanent failure. Although the swelling pressure for seven-day (short-term reactions) samples significantly decreased at 40 °C (Fig. 13a), the FSI did not fall below 10% in any blends. In contrast, superior outcomes in swelling reduction were found with increased

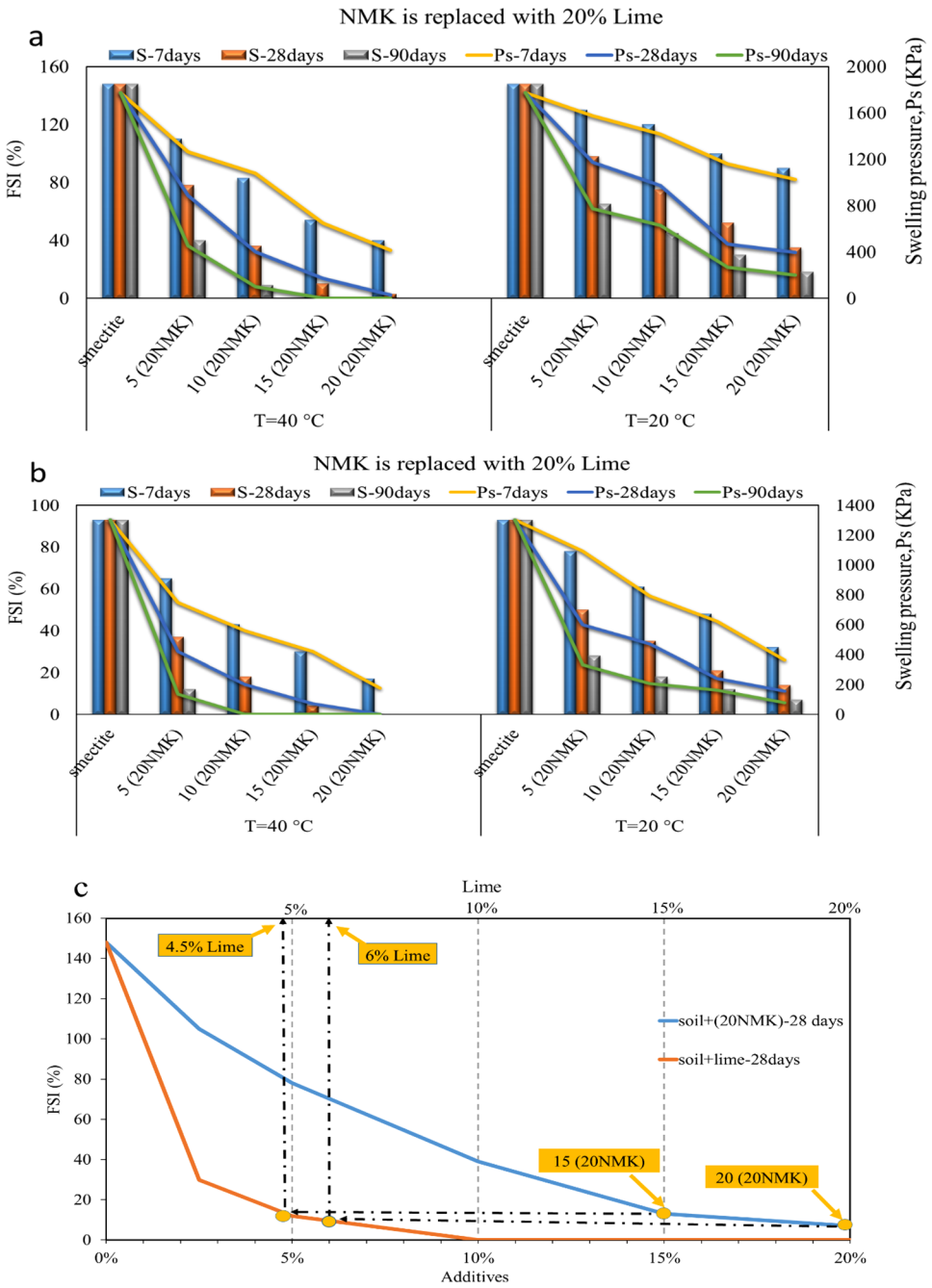

Fig. 13 FSI and swelling pressure of samples, after 7, 28, and 90 days, cured at 20 and 40 °C. **a** Without fibers; **b** With 1% PPFs; **C** The comparison of lime consumption in additives stabilized samples cured at 40 °C for 28 days with samples stabilized by sole lime

additive in 28 and 90-day samples and swelling pressure dramatically decreased.

For example, FSI of 15(20NMK) and 20(20NMK) after 28 days and also 10(20NMK), 15(20NMK), and 20(20NMK) after 90 days reached below 10%. Accordingly, it can be deduced that a large amount of additive cannot be entirely beneficial in mitigating soil expansion during a short period and need additional time to complete pozzolanic reactions.

On the other hand, at 20 °C (Fig. 13a), due to insufficient cementitious compounds for flocculation and agglomeration of particles, only the 20(20 NMK) sample after 90 days reduced FSI by less than 10%.

As illustrated in Fig. 13a, the FSI and swelling pressure diminish rapidly up to 28 days of curing at 40 °C and decrease with slight changes until the end of curing time. Therefore, it could be said that more CSH and CAH gels are quickly formed at higher temperatures to create a stronger and denser skeleton for limiting volumetric changes. This result is consistent with the findings of the EC test (Fig. 6), since decrease is notable at higher temperatures up to 28 days.

The significant result to reduce lime consumption is obtained from Fig. 13c. For example, by comparing the FSI curves of lime-soil samples with 15(20NMK) and 20(20NMK) containing 2.4 and 3.2% lime (see Table 5), it is clear that the effect of these blends on swelling reduction after 28 days of curing at 40 °C is equal to adding about 4.5 and 6% lime to the soil, respectively. It means that the volumetric changes can be restricted by less lime consumption (more than 45% reduction) which is a superior outcome in reducing lime usage, especially in stabilizing highly expansive soils.

The results in this section about reducing the content of lime consumption in swelling control to a vast extent are compatible with the UCS test results (sec "Effect of additives on the UCS test"). In general, by adding optimum compositions, smectite' tendency to swell declines due to three significant factors in non-fiber samples:

(i) The chemicals affect the reduction of interparticle forces, extend the capillary tension among the boundaries of the soil particles, and diminish the surface area of the clay particles to interact with water by creating a flocculent state.
(ii) In addition to the presence of GGBS, finer particles of NMK can provide more surface area of contact for the occurrence of chemical reactions with lime. As a consequence, further new cementing crystallines are produced in pozzolanic reactions, which are what bond the soil particles.
(iii) Nano-pores are filled due to the superfine NMK particles as excellent fillers. Consequently, a much denser and more uniform microstructure is created, reducing water absorption capacity.

To assess the effect of fibers on free swelling, Fig. 13b is given. Adding 1% of PPFs to specimens diminishes FSI and swelling pressure about 40 to 70%, which is added to the swelling reduction results of chemicals in Fig. 13a. Regarding the effect of higher curing temperature, the FSI of 10(20NMK), 15(20NMK), and 20(20NMK) samples after 28 days and all compounds after 90 days reached below 10% (Fig. 13b), and swelling pressure is significantly reduced. In contrast, the samples cured at 20 °C did not show such acceptable results.

The influence of reinforcers on swelling control increases with increasing additive concentration at early ages. The FSI of 5(20NMK) after seven days of curing before and after utilizing fibers is 110 and 65%, respectively, according to Fig. 13a, b at 40 °C (nearly 38% reduction). However, under the same curing conditions, for 20(20 NMK), it is 40 and 15%, respectively (almost 62.5% reduction).

Since longer curing time and a higher temperature accelerate the formation of cementitious gels, this factor improves the adherence among the particles, and the PPFs, which creates a better interaction among the components of the system and exhibits better performance in terms of swelling mitigation. In Fig. 13a, b at 40 °C, the FSI of 5(20NMK) before and after including fibers were 110 and 65% during seven days of curing (around 40% decrease), and in the 90-day sample, it reached 34 and 10%, respectively (about 70% decline).

Additionally, by incorporating fibers into the stabilized samples that were cured at lower temperatures, the unsatisfactory expansion-related flaws that result from less cementitious material formation can be corrected. For instance, swelling pressure of 20(20NMK) after seven days of curing at 20 °C, from 1068 in Fig. 13a (non-fibers), reached 410 kPa in the reinforced sample in Fig. 13b (approximately 62% reduction).

Finally, regarding swelling reduction mechanism of stabilized/reinforced samples, the following three reasons can be mentioned:

(i) The fibers operate as a spatial 3-D lattice, increase the interlocking density among the particles in the system, and create a unitary coherent matrix, resulting in a hindrance of swelling. [54].
(ii) PPFs with non-swelling features are replaced instead of smectite particles.
(iii) The strong connections of soil particles to fibers by adhesive products ameliorate particle packing and diminish the pores. Consequently, less water absorption occurs in the system.

In summary, it can be deduced that besides diminishing lime consumption, the S/R technique is beneficial for remediation purposes of expansive soils at the project site.

The Effect of Amendments on Ultrasonic Pulse Velocity

The velocity of compression stress waves can be measured in samples using a non-destructive technique by ultrasonic pulse velocity (UPV)[55]. The quickest path for a pulse to move through a material is directly related to its stiffness. The denser and stiffer the material, the higher the wave velocity. In contrast, UPV is lower in looser materials with large numbers of voids. Figure 0.14 shows the UPV values of stabilized/(un)reinforced samples.

According to the results, the wave velocity increases with rising additive's content. The highest UPV value among unreinforced samples is related to soil + 0(20NMK) and soil + 20(20NMK) for 7 and 28 days, respectively (Fig. 14a). This issue aligns with the results in Sects. " Effect of additives on the UCS test" and "Effect of additives on the Swell characteristics", which have indicated that the highest UCS value and the minimum FSI among all NMK replacements is related to 20% substitution after 28 days of curing at 40 °C. In fact, at 20% replacement, the production of more CSH and CAH gels results in a stronger, denser skeleton, which raises the UPV values.

According to Fig. 14b, reinforced specimens exhibit greater UPV values than specimens without fibers. The inclusion of PPFs with the contribution of cementitious gels enhances the integrity of sample structure, fills the voids, reduces porosity, and results in higher pulse velocity.

Moreover, increasing the period and temperature of curing is an essential factor to enhance wave velocity due to more formation of cement components and denser structures. This factor showed more effect, especially in reinforced samples (Fig. 16b).

The Relationships Between UCS and UPV Value

UPV technique can be used to control the effectiveness of the stabilization process. Accordingly, the best fits based on the data in Fig. 14c, d were performed to elucidate the numerical relationships between UCS and UPV results, which are indicated in the following equations:

$$UCS(\text{MPa}) = 0.0377e^{0.0038V\left(\frac{m}{s}\right)} \text{and} R^2 = 0.8776 \text{unreinforcedsamples} \quad (8)$$

$$UCS(\text{MPa}) = 0.0505e^{0.0035V\left(\frac{m}{s}\right)} \text{and} R^2 = 0.9042 \text{reinforcedsamples} \quad (9)$$

Equations 8 and 9 have a relatively acceptable correlation coefficient (R^2) and can be helpful for preliminary assessments. It should be emphasized that these correlations are valid and limited to properties of materials/mixtures and ranges of experimental results obtained.

Mineralogical and Microstructural Characteristics

Mineralogical Characteristics

XRD patterns for accurate assessment of smectite, 5%lime-soil, and the 20(20NMK) specimens after 28 days at 40 °C are presented in Fig. 15.

According to the results, the additives affect the specifications of XRD patterns, particularly the intensity related to the major d001-value of smectite. Thus, a significant reduction is seen in the major peak intensity associated with the reflection of montmorillonite mineral (i.e., d001-value = 12.4 Å) in smectite. This reduction can be ascribed to the formation of CAH (at 2θ about 11) and CSH (at 2θ about 29, 32, and 42) in long-term reactions.

According to the diffuse double layer (DDL) theory, when chemicals are added to soil, pore fluid is replaced with liquid that has a greater cation valence, and the thickness of the diffuse double layer tends to decrease. The thickness reduction causes the repulsive forces between the particles to diminish, and particles can get closer to forming a flocculated structure [18]. The aggregated particles have lower intensities due to a decrease in the reflections of the incident rays, which indicates a dense mass structure is generated compared to the initial unstabilized structure. Furthermore, due to the exhaustion of clay fractions during the long-term reactions, the reflections of montmorillonite mineral were reduced [56]. In fact, the appropriate ratio of NMK and GGBS in 20(20NMK) accelerates the hydration process. Due to the substantial SiO_2 and Al_2O_3 contents, the simultaneous presence of lime, NMK, and GGBS in the 20(20NMK) combination increase the CSH and CAH when compared to the 5% lime-soil sample. The release of Al_2O_3 in the chemical composition of NMK and GGBS led to the formation of CAH in 20(20NMK) mixture with intense reflection. Consequently, the solid phase bonding and densification in the system are improved which confirms higher strength and minor swelling of the optimum mixture.

On the other hand, more smectite fractions dissolve in the system when there is a balanced ratio of soluble ions present in the 20(20NMK). As a consequence, the montmorillonite mineral is associated with a greater drop in the peak intensities of the reflections.

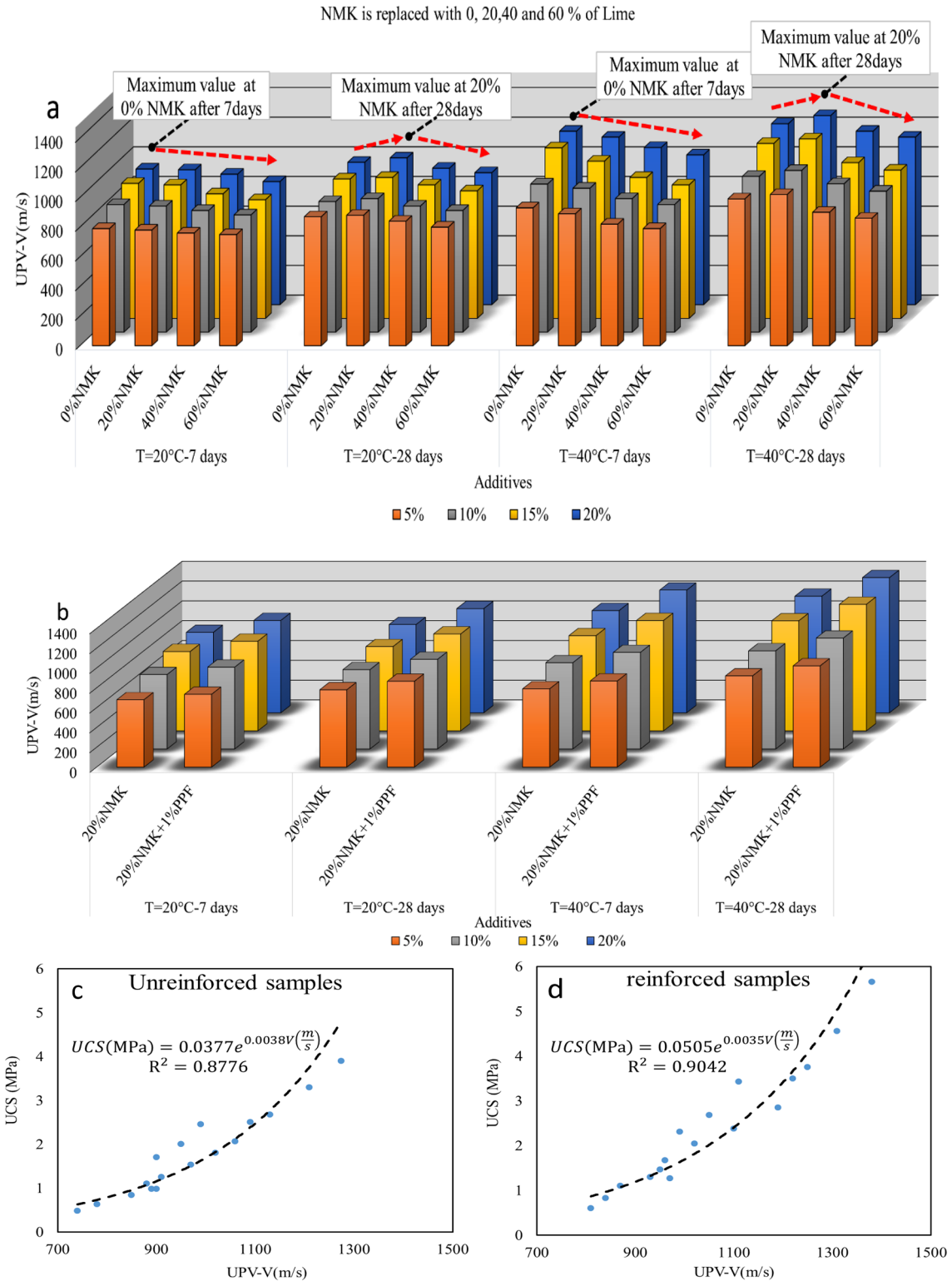

Fig. 14 The UPVvalue of samples cured at 20°and 40 °C for 7 and 28 days. **a** Without fibers; **b** 20% NMK replacement + 1% PPFs; **c** and **d** The UCS and UPV relationships for unreinforced/reinforced samples

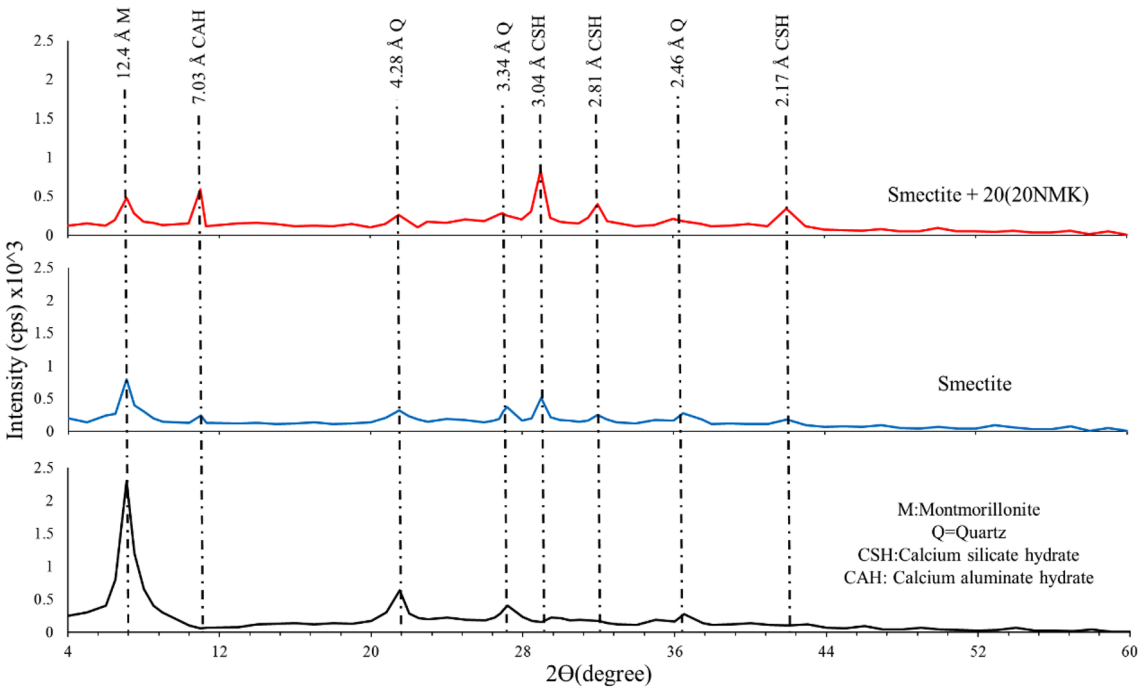

Fig. 15 XRD patterns for the smectite, smectite with 5% Lime, and smectite with 20(20NMK) samples after 28 days of treatment

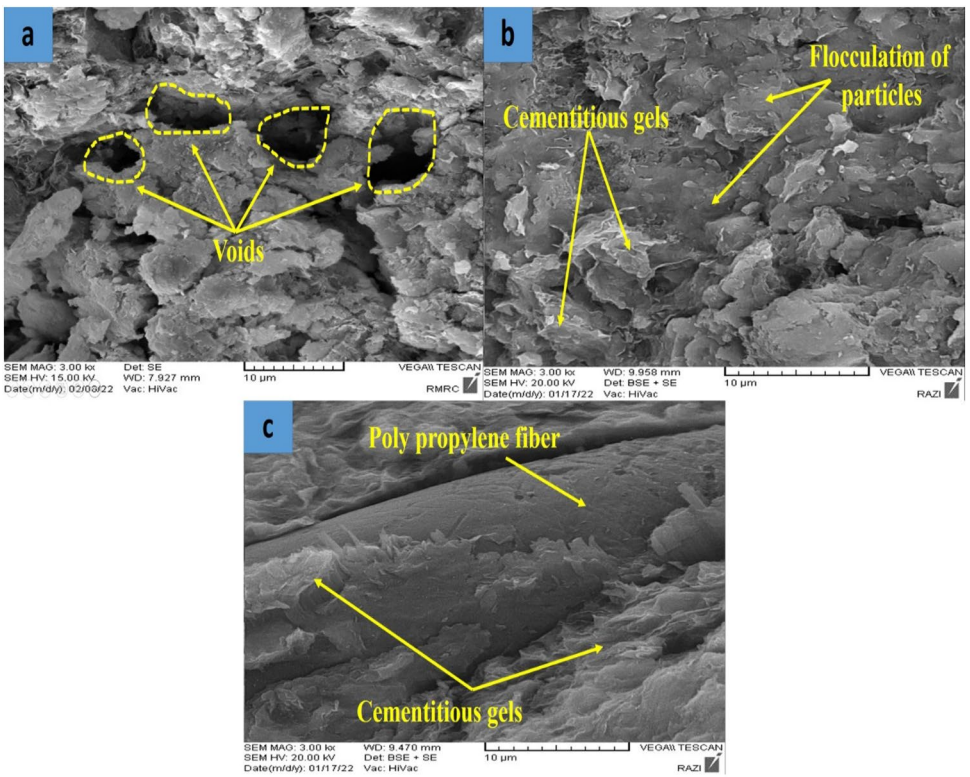

Fig. 16 SEM micrographs of samples after 28 days of curing at 40 °C. **a** Smectite; **b** Smectite with 20(20NMK); **c** Smectite with 20(20NMK) and 1% PPFs

Microstructural Characteristics

SEM results shown in Fig. 16 authenticate the laboratory test results and more effectively interpret microstructural changes in the sample. The images are provided to observe the microstructure of the smectite and the (un)reinforced 20(20NMK), cured after 28 days at 40 °C.

By comparing Fig. 16a, b, it is clear that the structure and texture of the treated specimen are different from those of smectite. The smectite has a discontinuous texture with apparent voids among the particles (Fig. 16a). On the contrary, the SEM result in Fig. 16b shows visual evidence of cementitious gel patches and flocculated structures after adding chemical materials. In fact, cementitious gels encapsulate the particles with a thin paste leading to a decline in water adsorption and soil swelling. Besides, they increase the soil particles' bonding strength and create dense packing of particles. This factor restricts the displacement of the particles in the stabilized samples. In other words, when the particles are bonded together by adhesive gels, they generate an integrated and dense structure. Therefore, the pores are diminished remarkably (Fig. 16b), improving strength and deformability characteristics [18].

As shown in Fig. 16c, cementitious gels adhere to soil particles and fibers, which causes the bond to strengthen, and more mobilized tensile forces are generated in fibers. Therefore, concurrent use of fibers and additives improves the UCS values and swelling potential due to better interactions between the fibers and particles. In general, fibers increase the integrity of samples in two ways:

On the one hand, fibers act as a bridge in place of cracks and prevent the increase of tensile crack width under swelling conditions and external compressive load. This function of fibers is known as "bridging effect" (Fig. 8 d).

On the other hand, when internal shear forces are generated in the samples due to external loading, the interlocking of the fibers' surfaces with nearby particles through adhesive gels has emerged as the confinement effect. This is a significant factor in restricting more microcracks extension and increasing samples' integrity.

Conclusion

This research studied the effectiveness of GGBS and NMK with lime as an activator on the engineering properties of smectite at various curing conditions in terms of macro and microstructure. Moreover, 1% PPFs were added to the optimum compounds to examine the concurrent effects of the stabilization/ reinforcement (S/R) technique. The results of this study can be used for a variety of projects, such as backfill of retaining walls, pavements, embankments, foundations, and slopes. Therefore, the most important conclusions that can be derived from this study are as follows:

1 Adding chemicals to the smectite increased EC and pH values at the beginning of the test. Higher temperature (40 °C), as a significant factor, accelerates the reactions. Accordingly, at 40 °C, the downward trend of the EC and pH values showed a higher rate over time. This issue confirms better-obtained results for improving strength and swelling characteristics for samples cured at 40 °C.
2 The ratio of lime to GGBS = 1:4, and replacing lime with 20% NMK as the optimum mixture showed the highest UCS values after 28 days of curing while the maximum compressive strength was obtained in 7-day samples without NMK. Longer curing time and rising temperature led to more formation of cementitious products that substantially raised the strength. Additives diminished the failure strain compared to smectite and led to brittle behavior. The strength of 28-day 20(20NMK) sample, despite a lower lime consumption (over 40% decline), was about 8.1 times that of smectite.
3 The inclusion of PPFs enhanced the strength by approximately 30 to 50% compared to the unreinforced samples. The longer curing time and rising temperature considerably affected the increasing strength of reinforced samples. Accordingly, the 28-day strength of the reinforced 20(20NMK) samples at 40 °C, despite a lower lime consumption (over 60% decline), was about 11.7 times that of smectite. Compared to the non-fibers samples, the failure strain increased, which converted brittleness into ductile behavior,
4 E_{50} and Eu followed an upward trend by increasing the percentage of the additive and curing temperature. Employing the fibers in the stabilized samples increased the ductility and required failure energy. As a result, compared to the non-fibers samples, Eu tended to increase, and E_{50} underwent a slight reduction.
5 FSI and swelling potential of smectite were reduced to minimum value by adding the optimum ratio of mixtures (lime to GGBS = 1:4 and replacing NMK with 20% lime). Moreover, the elapsed time to reach the ultimate heave was reduced despite an over 45% reduction in lime consumption. Higher temperatures exhibit better performance in terms of swelling mitigation in (un) reinforced samples. The strong connection between PPFs and particles through adhesive gels diminished the expansion of the reinforced sample about 40 to 70%. Rising additives content in fiber-reinforced specimens at early ages showed a positive effect on swelling control, in contrast to samples without fiber. At a lower

temperature, PPFs considerably improved the unsuitable performance in heave reduction.

6 According to the XRD pattern, the peak intensity of reflection related to the montmorillonite mineral was transformed into lower reflection by forming new CSH and CAH gels. SEM results confirmed the denser structure, fewer interparticle pores, and improved connections between particles and fibers through cementitious gels.

7 The 20% replacement of NMK showed higher UPV than other NMK substitutions. The inclusion of PPFs in stabilized specimens enhances the integrity of system and increases pulse velocity. The extended period and higher curing temperature were influential factors to increase UPV values.

Author Contributions MAPB**:** performing the experiments; analyzing the results and writing the preliminary text of the article. SHL, ARG: conceived and designed the experiments; checked the results of the tests; made improvement in interpretations. ARG , MAPB: help in interpreting test results; review and approval of tests; help in preparation of materials; help in determining the characteristics of materials to perform analysis; help in review of the figures. Finally, MAPB**,** SHL and ARG read the manuscript.

Funding This research did not receive any specifc grant from funding agencies in the public, commercial, or not-for-proft sectors.

Data Availability The datasets generated during and/or analysed during the current study are available from the corresponding author on reasonable request.

Declarations

Conflict of interest The authors declare no confict of interest.

References

1. Sarker D, Wang JX (2022) Moisture influence on structural responses of pavement on expansive soils. Transportation Geotechnics 35:100773
2. Marin-Lopez C et al (2022) The effect of the grain-size distribution on expansion and collapse behavior of expansive soils and their implications. Inter J Geosynthe Ground Eng 8(1):1–9
3. Jalal FE, Xu Y, Iqbal M, Javed MF, Jamhiri B (2021) Predictive modeling of swell-strength of expansive soils using artificial intelligence approaches: ANN, ANFIS and GEP. J Environ Manage 289:112420
4. Tiwari N, Satyam N (2021) Coupling effect of pond ash and polypropylene fiber on strength and durability of expansive soil subgrades: An integrated experimental and machine learning approach. J Rock Mechan Geotech Eng 13(5):1101–1112
5. Shenal Jayawardane V, Anggraini V, Emmanuel E, Yong LL, Mirzababaei M (2020) Expansive and compressibility behavior of lime stabilized fiber-reinforced marine clay,". J Materials Civil Eng 32(11):04020328
6. Reddy PS, Mohanty B, Rao BH (2020) Influence of clay content and montmorillonite content on swelling behavior of expansive soils. Inter J Geosynth Ground Eng 6(1):1–12
7. Jalal FE, Xu Y, Iqbal M, Jamhiri B, Javed MF (2021) Predicting the compaction characteristics of expansive soils using two genetic programming-based algorithms. Trans Geotech 30:100608
8. Hatmoko JT, Suryadharma H (2017) Shear behavior of calcium carbide residue-bagasse ash stabilized expansive soil. Procedia Eng 171:476–483
9. Barman D, Dash SK (2022) Stabilization of expansive soils using chemical additives: a review. J Rock Mechanics Geotech Eng 14(4):1319–1342
10. Jalal FE, Zahid A, Iqbal M, Naseem A, Nabil M (2022) Sustainable use of soda lime glass powder (SLGP) in expansive soil stabilization. Case Studies in Construction Materials 17:e01559
11. Charlie WA, Osman MA, Ali EM (1984) Construction on expansive soils in Sudan. J Constr Eng Manag 110(3):359–374
12. Al-Swaidani A, Hammoud I, Meziab A (2016) Effect of adding natural pozzolana on geotechnical properties of lime-stabilized clayey soil. J Rock Mechanics Geotech Eng 8(5):714–725
13. Maheepala M, Nasvi M, Robert D, Gunasekara C, Kurukulasuriya L (2022) A comprehensive review on geotechnical properties of alkali activated binder treated expansive soil. J Cleaner Prod 132488
14. Shi B, Jiang H, Liu Z, Fang H (2002) Engineering geological characteristics of expansive soils in China. Eng Geol 67(1–2):63–71
15. Behnood A (2018) Soil and clay stabilization with calcium-and non-calcium-based additives: a state-of-the-art review of challenges, approaches and techniques. Transport Geotech 17:14–32
16. Sakr MA, Azzam WR, Meguid MA, Hassan AF, Ghoneim HA (2021) Enhancing the swelling characteristics and shear strength of expansive soil using ferric chloride solution. Inter J Geosynth Ground Eng 7(4):1–9
17. Jalal FE, Xu Y, Jamhiri B, Memon SA (2020) On the recent trends in expansive soil stabilization using calcium-based stabilizer materials (CSMs): a comprehensive review. Adv Mater Sci Eng 2020:1–23
18. Goodarzi AR, Akbari HR, Salimi M (2016) Enhanced stabilization of highly expansive clays by mixing cement and silica fume. Appl Clay Sci 132:675–684
19. Khadka SD, Jayawickrama PW, Senadheera S, Segvic B (2020) Stabilization of highly expansive soils containing sulfate using metakaolin and fly ash based geopolymer modified with lime and gypsum. Transportation Geotechnics 23:100327
20. Al-Mukhtar M, Lasledj A, Alcover J-F (2010) Behaviour and mineralogy changes in lime-treated expansive soil at 20 C. Appl Clay Sci 50(2):191–198
21. Al-Mukhtar M, Lasledj A, Alcover J-F (2010) Behaviour and mineralogy changes in lime-treated expansive soil at 50° C. Appl Clay Sci 50(2):199–203
22. De Windt L, Deneele D, Maubec N (2014) Kinetics of lime/bentonite pozzolanic reactions at 20 and 50 C: Batch tests and modeling. Cem Concr Res 59:34–42
23. Akbari HR, Sharafi H, Goodarzi AR (2021) Effect of polypropylene fiber inclusion in kaolin clay stabilized with lime and nanozeolite considering temperatures of 20 and 40 C. Bull Eng Geol Env 80(2):1841–1855
24. Salimi M, Ghorbani A (2020) Mechanical and compressibility characteristics of a soft clay stabilized by slag-based mixtures and geopolymers. Appl Clay Sci 184:105390
25. Syed M, GuhaRay A (2020) Effect of fiber reinforcement on mechanical behavior of alkali-activated binder-treated expansive soil: reliability-based approach. Int J Geomech 20(12):04020225
26. Rabbani P, Tolooiyan A, Lajevardi SH, Daghigh Y, Falah M (2019) The effect of the depth of cutter soil mixing on the

compressive behavior of soft clay treated by alkali-activated slag. KSCE J Civ Eng 23(10):4237–4249
27. Chenarboni HA, Lajevardi SH, MolaAbasi H, Zeighami E (2021) The effect of zeolite and cement stabilization on the mechanical behavior of expansive soils. Constr Build Mater 272:121630
28. Dang LC, Khabbaz H, Ni B-J (2021) Improving engineering characteristics of expansive soils using industry waste as a sustainable application for reuse of bagasse ash. Transport Geotech 31:100637
29. Jafari SH, Lajevardi SH, Sharifipour M, Kamalian M (2021) Evaluation of small strain stiffness characteristics of soft clay treated with lime and nanosilica and correlation with UCS (qu). Bull Eng Geol Env 80(4):3163–3175
30. Heidarizadeh Y, Lajevardi SH, Sharifipour M (2021) Correlation between small-strain shear stiffness and compressive strength of clayey soils stabilized with cement and Nano-SiO2. Inter J Geosyn Ground Eng 7(1):1–12
31. Arora A, Singh B, Kaur P (2019) Performance of Nano-particles in stabilization of soil: a comprehensive review. Mater Today 17:124–130
32. Eyo EU, Ng'ambi S, Abbey S (2020) Incorporation of a nanotechnology-based additive in cementitious products for clay stabilisation. J Rock Mechanics Geotech Eng 12(5):1056–1069
33. Yao K, Wang W, Li N, Zhang C, Wang L (2019) Investigation on strength and microstructure characteristics of nano-MgO admixed with cemented soft soil. Constr Build Mater 206:160–168
34. Kumar A, Sinha S (2023) Role of multiwalled carbon nanotube in the improvement of compaction and strength characteristics of fly ash stabilized soil. Int J Pavement Res Technol 1–22
35. Zoriyeh H, Erdem S, Gürbüz E, Bozbey İ (2020) Nano-clay modified high plasticity soil as a building material: Micro-structure linked engineering properties and 3D digital crack analysis. J Building Eng 27:101005
36. Norhasri MM, Hamidah M, Fadzil AM, Megawati O (2016) Inclusion of nano metakaolin as additive in ultra high performance concrete (UHPC). Constr Build Mater 127:167–175
37. Xie J et al (2020) Effect of nano metakaolin on compressive strength of recycled concrete. Constr Build Mater 256:119393
38. Jiang N-J, Du Y-J, Liu K (2018) Durability of lightweight alkali-activated ground granulated blast furnace slag (GGBS) stabilized clayey soils subjected to sulfate attack. Appl Clay Sci 161:70–75
39. Goodarzi AR, Movahedrad M (2017) Stabilization/solidification of zinc-contaminated kaolin clay using ground granulated blast-furnace slag and different types of activators. Appl Geochem 81:155–165
40. Moghal AAB, Chittoori BC, Basha BM (2018) Effect of fibre reinforcement on CBR behaviour of lime-blended expansive soils: reliability approach. Road Materials Pavement Design 19(3):690–709
41. Moghal AAB, Chittoori BC, Basha BM, Al-Mahbashi AM (2018) Effect of polypropylene fibre reinforcement on the consolidation, swell and shrinkage behaviour of lime-blended expansive soil. Int J Geotech Eng 12(5):462–471
42. Tiwari N, Satyam N, Patva J (2020) Engineering characteristics and performance of polypropylene fibre and silica fume treated expansive soil subgrade. Inter J Geosynth Ground Eng 6(2):1–11
43. Akbari HR, Sharafi H, Goodarzi AR (2021) Effect of polypropylene fiber and nano-zeolite on stabilized soft soil under wet-dry cycles. Geotext Geomembr 49(6):1470–1482
44. Wei L, Chai S, Xue M, Wang P, Li F (2022) Structural damage and shear performance degradation of fiber–lime–soil under freeze–thaw cycling. Geotext Geomembr 50(5):845–857
45. Dhar S, Hussain M (2019) The strength behaviour of lime-stabilised plastic fibre-reinforced clayey soil. Road Materials Pavement Design 20(8):1757–1778
46. Vakili AH, Ghasemi J, bin Selamat MR, Salimi M, Farhadi MS (2018) Internal erosional behaviour of dispersive clay stabilized with lignosulfonate and reinforced with polypropylene fiber. Constr Build Mater 193:405–415
47. Syed M, GuhaRay A, Agarwal S, Kar A (2020) Stabilization of expansive clays by combined effects of geopolymerization and fiber reinforcement. J Inst Eng (India): Series A 101(1):163–178
48. Abdi MR, Ghalandarzadeh A, Chafi LS (2021) An investigation into the effects of lime on compressive and shear strength characteristics of fiber-reinforced clays. J Rock Mechanics Geotech Eng 13(4):885–898
49. Yi Y, Gu L, Liu S (2015) Microstructural and mechanical properties of marine soft clay stabilized by lime-activated ground granulated blastfurnace slag. Appl Clay Sci 103:71–76
50. Chowdary B, Ramanamurty V, Pillai RJ (2020) Fiber reinforced geopolymer treated soft clay–An innovative and sustainable alternative for soil stabilization. Mater Today 32:777–781
51. Zhang J, Deng A, Jaksa M (2021) Enhancing mechanical behavior of micaceous soil with jute fibers and lime additives. J Rock Mechanics Geotech Eng 13(5):1093–1100
52. Miraki H, Shariatmadari N, Ghadir P, Jahandari S, Tao Z, Siddique R (2022) Clayey soil stabilization using alkali-activated volcanic ash and slag. J Rock Mechanics Geotech Eng 14(2):576–591
53. Chaduvula U, Viswanadham B, Kodikara J (2022) Centrifuge model studies on desiccation cracking behaviour of fiber-reinforced expansive clay. Geotext Geomembr 50(3):480–497
54. Soltani A, Deng A, Taheri A (2018) Swell–compression characteristics of a fiber–reinforced expansive soil. Geotext Geomembr 46(2):183–189
55. Boz A, Sezer A (2018) Influence of fiber type and content on freeze-thaw resistance of fiber reinforced lime stabilized clay. Cold Reg Sci Technol 151:359–366
56. Goodarzi AR, Salimi M (2015) Stabilization treatment of a dispersive clayey soil using granulated blast furnace slag and basic oxygen furnace slag. Appl Clay Sci 108:61–69
57. Sharma AK, Sivapullaiah P (2017) Swelling behaviour of expansive soil treated with fly ash–GGBS based binder. Geomechanics Geoengineering 12(3):191–200
58. Mohanty S, Roy N, Singh SP, Sihag P (2021) Strength and durability of flyash, GGBS and cement clinker stabilized dispersive soil. Cold Reg Sci Technol 191:103358
59. Zhang T, Yue X, Deng Y, Zhang D, Liu S (2014) Mechanical behaviour and micro-structure of cement-stabilised marine clay with a metakaolin agent. Constr Build Mater 73:51–57
60. Rajabi AM, Hamrahi Z (2021) An experimental study on the influence of metakaolin on mechanical properties of a clayey sand. Bull Eng Geol Env 80(10):7921–7932